Remote Sensing of Environment 247 (2020) 111949

Contents lists available at ScienceDirect

Remote Sensing of Environment

journal homepage: www.elsevier.com/locate/rse

Changes of water clarity in large lakes and reservoirs across China observed from long-term MODIS

Shenglei Wang[a,b], Junsheng Li[b,c], Bing Zhang[b,c,*], Zhongping Lee[d], Evangelos Spyrakos[e], Lian Feng[f], Chong Liu[g], Hongli Zhao[h], Yanhong Wu[b], Liping Zhu[g], Liming Jia[i], Wei Wan[a], Fangfang Zhang[b], Qian Shen[b], Andrew N. Tyler[e], Xianfeng Zhang[a]

[a] School of Earth and Space Sciences, Peking University, Beijing, China
[b] Key Laboratory of Digital Earth Science, Aerospace Information Research Institute, Chinese Academy of Sciences, Beijing, China
[c] University of Chinese Academy of Sciences, Beijing, China
[d] School for the Environment, University of Massachusetts Boston, Boston, MA, USA
[e] Biological and Environmental Sciences, Faculty of Natural Sciences, University of Stirling, Stirling, UK
[f] State Environmental Protection Key Laboratory of Integrated Surface Water-Groundwater Pollution Control, School of Environmental Science and Engineering, Southern University of Science and Technology, Shenzhen, China
[g] Key Laboratory of Tibetan Environment Changes and Land Surface Processes, Institute of Tibetan Plateau Research, Chinese Academy of Sciences, Beijing, China
[h] China Institute of Water Resources and Hydropower Research, Beijing, China
[i] Environmental Monitoring Central Station of Heilongjiang Province, Harbin, China

ARTICLE INFO

Keywords:
Secchi disk depth
Lakes and reservoirs
MODIS
FUI
Hue angle
Water clarity changes

ABSTRACT

Water clarity is a well-established first-order indicator of water quality and has been used globally by water regulators in their monitoring and management programs. Assessments of water clarity in lakes over large temporal and spatial scales, however, are rare, limiting our understanding of its variability and the driven forces. In this study, we developed and validated a robust Secchi disk depth (Z_{SD}) algorithm for lakes across China based on two water color parameters, namely Forel-Ule Index (FUI) and hue angle α, retrieved from MODIS data. The MODIS Z_{SD} model shows good results when compared with in-situ measurements from 17 lakes, with a 27.4% mean relative difference (MRD) in the validation dataset. Compared with other empirical Z_{SD} models, our FUI and α-based model demonstrates improved performance and adaptability over a wide range of water clarity and trophic states. This algorithm was subsequently applied to MODIS measurements to provide a comprehensive assessment of water clarity in large lakes (N = 153) across China for the first time. The mean summer Z_{SD} of the studied lakes between 2000 and 2017 demonstrated marked spatial and temporal variations. Spatially, the Z_{SD} of large lakes presented a distinct spatial pattern of "high west and low east" over China. This spatial pattern was found to be associated with the significant differences in lake depth and altitude between west and east China while China's population, GDP, temperature, and precipitation distribution have also contributed to a certain extent. Temporally, the Z_{SD} of most lakes increased during this period, with an overall mean rate of 3.3 cm/yr for all lakes. Here, 38.6% (N = 59) of the lakes experienced a significant increase in their Z_{SD} value during the past 18 years while only 8.5% (N = 13) showed a significant decreasing trend. Significant increases in lake Z_{SD} were observed in west China, which were found to correlate with the increase of air temperature and lake surface area. This is possibly a response of the lakes in west China to climate change. In the lake systems of east China, which are predominately used as a drinking water source, the increase in lake Z_{SD} was found to be strongly correlated with changes in local GDP (gross domestic production), NDVI (normalized difference vegetation index) and lake surface area, suggesting a combined effect of the implemented management practices and climatic variability. The results of this study provide important information for water quality conservation and management in China, and also highlight the value of satellite remote sensing in monitoring water quality over lakes at a large scale and long-term.

* Corresponding author at: Key Laboratory of Digital Earth Science, Aerospace Information Research Institute, Chinese Academy of Sciences, No. 9 Dengzhuang South Road Haidian District, Beijing 100094, China.
E-mail address: zb@radi.ac.cn (B. Zhang).

https://doi.org/10.1016/j.rse.2020.111949
Received 13 August 2019; Received in revised form 4 June 2020; Accepted 8 June 2020
Available online 27 June 2020

1. Introduction

Lakes and reservoirs are critical for our wellbeing since they are core to water supply, food production, recreation activities, commerce, and human health (Dörnhöfer and Oppelt, 2016; Williamson et al., 2009; Tyler et al., 2016). However, these inland water bodies are faced with multiple and compounding pressures from a number of users and uses, as well as climate change (Adrian et al., 2009; de Eyto et al., 2016; O'Reilly et al., 2003). Water clarity provides important and synthetic information on water quality and lake's ecosystem status (Kirk, 1994; McCullough et al., 2012; Pirhalla et al., 2017). It varies with the three major optically active components (OAC) of water, i.e., suspended particulate matter (SPM), phytoplankton (usually represented by chlorophyll-a concentration, Chl-a), and colored dissolved organic matter (CDOM). Water clarity has a direct link to the underwater light field and therefore to lake photosynthetic production (Biber et al., 2005; McPherson et al., 2011). Water clarity monitoring is essential to understand long-term changes in lake ecosystems, as well as to support environmental protection strategies (Olmanson et al., 2008; Suominen and Tolvanen, 2016).

Water clarity has been historically measured in water bodies as the Secchi disk depth (Z_{SD}, m), which is determined by the depth at which a white or black and white disk disappears from the observer's sight (Lee et al., 2018a, 2018b; Wernand, 2010). Compared with other measures of water clarity, e.g., the turbidity or downwelling irradiance diffuse attenuation coefficient (K_d), the collection of Secchi disk depth is much easier and more cost-effective. Therefore, the Z_{SD} measurement has been performed extensively with a tradition still ongoing and expanding by numerous citizen science projects, such as the Secchi Disk and Eye on Water (http://www.secchidisk.org/;https://www.eyeonwater.org/).

Although the Z_{SD} is one of the simplest measures of water properties, information on water clarity is still limited in terms of spatial coverage, temporal frequency, and representativeness. Given the revisit capacities and wide-swath observation (Doron et al., 2011; Mouw et al., 2015) of sensors onboard satellite platforms, Earth observation (EO) data can provide a feasible source to monitor long-term changes in water clarity over large regions. Numerous empirical models have been developed to estimate water clarity, including single-band and band-ratio algorithms. For example, Olmanson et al. (2008) developed and evaluated an empirical Z_{SD} model using Landsat TM1 and TM3 bands to monitor 20-year changes of Z_{SD} over 10,500 lakes in the state of Minnesota. They demonstrated that satellite imagery can provide an accurate method to obtain comprehensive spatial and temporal coverage of water clarity. In another study, Binding et al. (2007, 2015) produced monthly binned images of remote sensing radiance over the Great Lakes by merging data from the Coastal Zone Color Scanner (CZCS), the Sea-viewing Wide Field-of-view Sensor (SeaWiFS), and the Moderate Resolution Imaging Spectroradiometer (MODIS). They used the remote sensing radiance at 555 nm to interpret changes in the Z_{SD} across the Great Lakes. Duan et al. (2009) evaluated the Z_{SD} of three lakes in northeast China from Landsat TM imagery based on four regression equations, which indicated strong geographic patterns in lake water clarity over this region.

The theoretical interpretation of Z_{SD} has been recently revised by considering a Secchi disk not a point source to human eyes (Lee et al., 2015; Lee et al., 2018a, 2018b), which led to an innovative semi-analytical model for estimating Z_{SD} from satellite imagery via deriving water's inherent optical properties (IOPs) (Lee et al., 2016). Rodrigues et al. (2017) evaluated this new model in a reservoir in Brazil with Landsat-8 OLI and Sentinel-2 MSI data, and suggested that the derivation of IOPs was the limiting factor in retrieving accurate Z_{SD} by this model. Feng et al. (2019a) tested and applied this new model to explore changes in lake clarity in the Middle and Lower Yangtze River basin in China, and analyzed the environmental factors affecting the change trends. Nevertheless, the complexity and dynamic variability of optical properties found in inland waters (Spyrakos et al., 2018) remain as obstacles for the systematic application of these empirical and analytical models over a wider range of optical water types (Ren et al., 2018). Moreover, challenges associated with atmospheric correction, adjacency effects, low signal-to-noise and limited resolutions of existing sensors over lakes can exacerbate these difficulties (Li et al., 2017; Mouw et al., 2015; Palmer et al., 2015; Wang et al., 2011).

There are thousands of lakes and reservoirs (hereafter termed as "lakes" for brevity) located broadly in China characterized by a variety of diverse types and regional characteristics (Ma et al., 2011; Wang and Dou, 1998). Based on the geological origin, topography, water resource characteristics, and lake hydrological characteristics, Chinese lakes can be divided into five distinct regions, i.e., the Qinghai-Tibet Plateau Region (QTR), Mengxin Plateau Region (MXR), Yungui Plateau Region (YGR), Northeast Mount-Plain Region (NER), and East Plain Region (EPR) (Wang and Dou, 1998). In the recent half-century, China has experienced rapid economic development and population expansion, as well as the effects of climate change, which collectively has placed pressure on lake ecosystems (Ma et al., 2010; Yang et al., 2010a, 2010b; Zhang et al., 2019). Effective monitoring of lake clarity across large areas and long-time spans is an important task for government management agencies. Given the difficulties in Z_{SD} estimation over various types of optically complex inland waters, a comprehensive and systematic assessment of water clarity in lakes across China has not yet been completed.

In recent years, the FUI (Forel-Ule Index) and hue angle (α) have been shown to be useful water color parameters in indicating the bulk changes of water quality, and can be derived from multispectral satellite data with high accuracies (Van der Woerd and Wernand, 2018; Wang et al., 2015). Recent studies have found that there are strong correlations between Z_{SD} and FUI for both oceanic and inland waters (Garaba et al., 2015; Li et al., 2016; Pitarch et al., 2019; Wernand et al., 2013). In this study, we developed an empirical Z_{SD} model based on FUI and α and evaluated it using a comprehensive match-up dataset collected from geographically widespread lakes distributed across China. Further, for the first time, maps of Z_{SD} for nationwide large lakes in China were generated based on MODIS observations and used to reveal the long-term temporal and spatial trends in water clarity across China from 2000 to 2017. Moreover, the relationship between the lake clarity and economic developments and climate change over different regions were explored and discussed.

2. Data acquisition

2.1. MODIS data

MODIS surface reflectance products (MOD09) provide an estimate of the surface spectral reflectance for Bands 1–7 (i.e., 645, 859, 469, 555, 1240, 1640, and 2130 nm) at a spatial resolution of 500 m (Vermote, 2015). As global products started from 2000, MOD09 products are considered an important data source for long-term and large scale environmental monitoring (Feng et al., 2018a; Hou et al., 2017). MOD09A1 is the 8-day composite surface reflectance data, which selects one best reflectance observation during the 8-day period at the pixel level with the criteria including cloud free and optimal solar zenith (Vermote and Kotchenova, 2008). Hence, this MOD09A1 data were used to estimate the long-term Z_{SD} changes in large lakes across China in this study. In order to narrow the match-up time window, the daily MOD09 data (MOD09GA) were used to match the in-situ data and develop the model after removing the pixels containing clouds and other obvious noises. The daily MOD09GA data were not used in the long-term monitoring in this study because it may contain large errors and even negative reflectance over lakes that are probably caused by bad observational conditions and non-optimal atmospheric corrections, while the 8-day composite MOD09A1 data can avoid these uncertainties in a certain degree by selecting the best observation for each

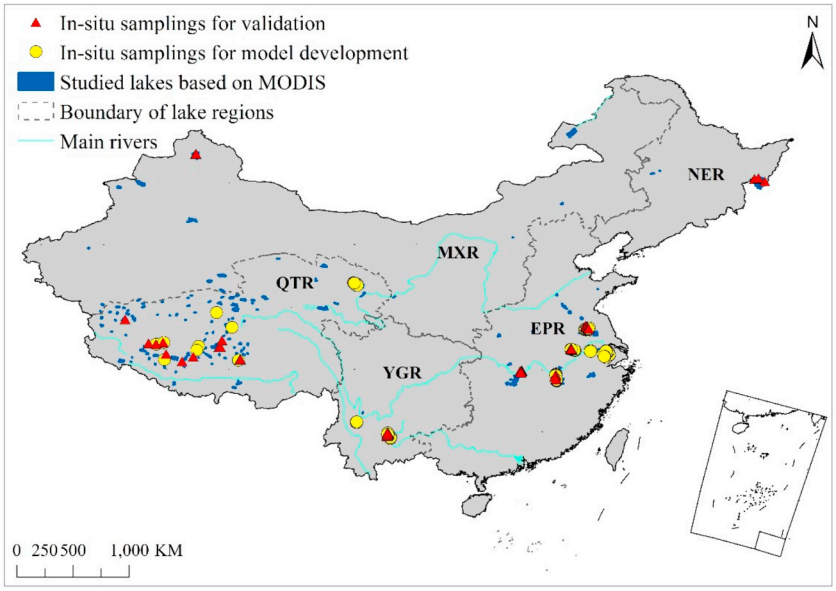

Fig. 1. Locations of the in-situ sampling sites for model development (N = 183) and validation (N = 105) and MODIS studied lakes (N = 153) in the five lake regions (shown in bold on the map) across China.

pixel. The image archive between 2000 and 2017 was downloaded from the Goddard Space Flight Center (GSFC) of the National Aeronautics and Space Administration (NASA).

2.2. In-situ and simulated datasets

A large dataset of in-situ Z_{SD} including 478 samplings was collected from 27 lakes across China during 38 campaigns from 2006 to 2019 and compiled to develop and test the Z_{SD} estimation model in this study (see Fig. 1). The Z_{SD} values in our dataset ranged between 0.1 and 13.1 m. A variety of conditions and characteristics were found in the dataset ranging from the clear and oligotrophic lakes in the Qinghai-Tibet Plateau in west China, such as Qinghai Lake and Namco Lake, to the turbid and eutrophic lakes in the middle and lower reaches of the Yangtze River in east China, such as Taihu Lake and Chaohu Lake, and to eutrophic lake in southwest China, i.e., Dianchi Lake. Due to the remoteness, altitude, and harsh conditions that characterize the Qinghai-Tibet Plateau, fewer data were collected from lakes in this area where Z_{SD} values are typically higher. We note a majority of the in-situ data in the QTR were acquired from Liu et al. (2017). For these measurements, a typical black and white Secchi disk was used in the field campaigns to determine Z_{SD}. The disk was lowered into the water and the Z_{SD} was determined as the depth where the disk was no longer visible by an observer from the water surface. To avoid the effects of land-adjacency and low solar altitude, in situ samples were collected at least 500 m away from the shoreline and around solar noon time.

The in-situ measured Z_{SD} data were matched up with daily MOD09GA data with the purpose of developing an empirical model to estimate Z_{SD} using the MOD09 images. The nearest pixel to the in-situ sampling sites was obtained under the condition that the pixel was not detected as clouds, ice, snow, and other potential noises. The spatial variability of the match-up pixel was also checked at 555 nm with the criteria that the coefficient of variation (CV) is less than 0.2 within a 3 * 3 pixel-box centered at the match-up pixel (Zibordi et al., 2009). In total, there were 288 match-up pairs between Z_{SD} and MOD09GA data compiled from the totally 476 samplings in the 27 lakes (Table 1). With the match-up pairs, 183 data pairs (64% of the total) from 20 campaigns were used to develop the Z_{SD} model, while an independent dataset, including 105 data pairs (36% of the total) from 18 independent campaigns with a wide range of Z_{SD}, was used to test the model (see Table 1). Besides, following the protocol described in Mueller et al. (2003), in-situ measured remote sensing reflectance (R_{rs}, sr^{-1}) data were also collected in 246 of the 476 samplings, mainly from Lake Taihu, Lake Chaohu, Lake Poyang, Lake Dianchi and Lake Qinghai. This in-situ R_{rs} and Z_{SD} dataset was used to further evaluate the proposed Z_{SD} model through comparing with other Z_{SD} estimation models.

In addition to the in-situ dataset, a Hydrolight simulated dataset (IOCCG, 2006), consisting of 500 data points, was employed in the step of Z_{SD} model development. In this simulated dataset, apparent optical properties (AOPs), including the hyperspectral $R_{rs}(\lambda)$ were generated by the Hydrolight code using the input inherent optical properties (IOPs) in a wide range. More details about this dataset can be found in IOCCG (2006). The FUI in this dataset was calculated from $R_{rs}(\lambda)$ after conversion to MODIS bands using the MODIS relative spectral response (RSR). The Z_{SD} of each simulation was derived following the method described in Lee et al. (2018a, 2018b). The Z_{SD} values ranged from 0.8 to 34.0 m, with an average of 9.1 m.

2.3. Environmental factors

To better understand the potential environmental factors that may contribute to the spatial and long-term variability of lake clarity in China, three different categories of environmental factors, which have been identified as influencing factors of water quality in previous studies (Feng et al., 2019a; Meng et al., 2015; Srebotnjak et al., 2012; Zhou et al., 2012), were considered and preliminarily examined: (1) lake geographic factors (i.e., lake altitude (AL), surface area (SA), average water depth (WD), and local normalized difference vegetation index (NDVI)), (2) meteorological factors (i.e., near surface air temperature (AT), precipitation (PR), and wind speed (WS)), and (3) human activity factors (i.e., local population (PO) and gross domestic production (GDP)).

AL data for the lakes were acquired from global digital elevation model (DEM) data produced by the NASA Shuttle Radar Topography Mission (Farr et al., 2007). WD data for 46 of the studied lakes across the different lake regions were the average lake depths acquired from Wang and Dou (1998). Annual SA data for the lakes were retrieved from the water segmentation of MOD09A1 data used in this study. Annual NDVI data were acquired as the monthly MODIS vegetation product, e.g., MOD13A3, provided by LAADS DAAC at the NASA Goddard Space Flight Center. Monthly AT, PR and WS data were the surface temperature, precipitation and wind speed data with a

Table 1
Lake name, location, the total number of samplings (N1), the number of in-situ R_{rs} samplings (N2), the number of match-ups(N3), sampling date (Date) and Z_{SD} ranges of the in-situ data collection campaigns (campaigns for model development are given in bold while the independent campaigns for model testing are given in italics).

Campaign No.	Lake name	Lat. (N)	Long. (E)	Lake region	N1	N2	N3	Date	Z_{SD} ranges (m)
1	Taihu	30.2	120.1	EPR	50	46	23	2006.01	0–1
2	Taihu	30.2	120.1	EPR	50	39	34	2006.07	0–1
3	Taihu	30.2	120.1	EPR	50	43	6	2006.10	0–1
4	Taihu	30.2	120.1	EPR	50	49	37	2007.01	0–1
5	Chaohu	31.5	117.5	EPR	33	24	5	2009.06	0–1
6	Hongze	33.3	118.8	EPR	27	–	20	2015.05	0–1
7	Poyang	29.1	116.1	EPR	28	22	10	2011.07	0–1
8	Shijiu	31.5	118.9	EPR	6	–	3	2018.07	0–1
9	Dianchi	24.8	102.7	YGR	8	8	4	2009.12	0–1
10	Erhai	25.8	100.2	YGR	10	–	7	2015.10	1–2
11	Fuxian	24.5	102.9	YGR	12	–	11	2015.10	> 2
12	Dongco[1]	32.2	84.8	QTR	1	–	1	2012.08	0–1
13	Dogai Coring[1]	34.6	89.0	QTR	1	–	1	2016.11	1–2
14	Qinghai	36.8	100.2	QTR	17	15	15	2014.08	2–5
15	Zhangnaico[1]	31.6	87.4	QTR	1	–	1	2012.08	2–5
16	Migriggyangzhamco[1]	33.4	90.2	QTR	1	–	1	2016.1	2–5
17	Lagkorco[1]	32.0	84.2	QTR	1	–	1	2012.08	2–5
18	Dazeco[1]	31.9	87.6	QTR	1	–	1	2012.8	> 5
19	Yunboco[1]	30.8	84.8	QTR	1	–	1	2012.08	> 5
20	Namco[1]	30.7	90.6	QTR	1	–	1	2016.11	> 5
21	*Xingkai*	*45.2*	*132.5*	*NER*	*3*	–	*3*	*2014.06*	*0–1*
22	*Xingkai*	*45.2*	*132.5*	*NER*	*3*	–	*2*	*2014.07*	*0–1*
23	*Honghu*	*29.8*	*113.3*	*EPR*	*20*	–	*9*	*2019.03*	*0–1*
24	*Hongze*	*33.3*	*118.6*	*EPR*	*12*	–	*12*	*2014.04*	*0–1*
25	*Chaohu*	*31.5*	*117.5*	*EPR*	*13*	–	*12*	*2013.09*	*0–1*
26	*Dianchi*	*24.8*	*102.7*	*EPR*	*40*	–	*37*	*2017.11*	*0–1*
27	*Poyang*	*29.1*	*116.1*	*EPR*	*12*	–	*10*	*2009.10*	*0–1*
28	*Ngangzeco*	*31.0*	*87.1*	*QTR*	*1*	–	*1*	*2018.09*	*1–2*
29	*Pusaier*	*32.3*	*89.4*	*QTR*	*1*	–	*1*	*2017.07*	*1–2*
30	*Ulungur*	*47.2*	*87.3*	*MXR*	*5*	–	*3*	*2015.07*	*2–5*
31	*Dawaco*	*31.2*	*85.0*	*QTR*	*1*	–	*1*	*2018.09*	*2–5*
32	*Dongco*	*32.2*	*84.8*	*QTR*	*1*	–	*1*	*2018.09*	*2–5*
33	*Camco*	*32.1*	*83.5*	*QTR*	*1*	–	*1*	*2018.09*	*2–5*
34	*Namco*	*30.7*	*90.6*	*QTR*	*5*	–	*4*	*2017.08*	*> 5*
35	*Silingco*	*31.8*	*88.9*	*QTR*	*4*	–	*4*	*2017.07*	*> 5*
36	*Lagkorco*	*32.0*	*84.1*	*QTR*	*2*	–	*2*	*2018.09*	*> 5*
37	*Lumajangdongco*	*34.0*	*81.6*	*QTR*	*2*	–	*1*	*2018.09*	*> 5*
38	*Monco Bunnyi*	*30.7*	*86.2*	*QTR*	*1*	–	*1*	*2018.09*	*> 5*

[1] Note: these in-situ data in the QTR were acquired from Liu et al. (2017).

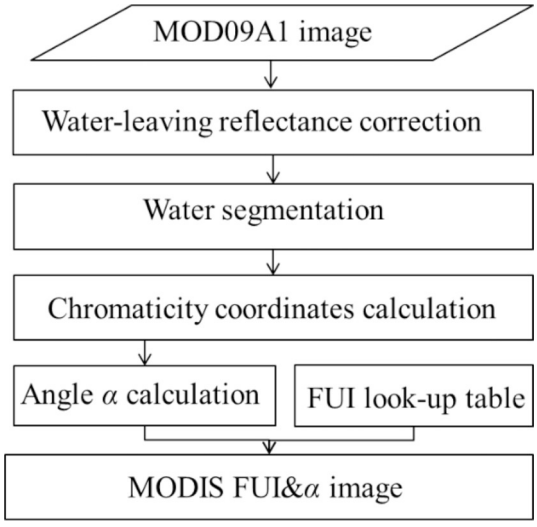

Fig. 2. A flowchart of the MODIS preprocessing steps and the calculation of FUI and α.

resolution of 0.1 degree from China meteorological forcing dataset (CMFD) which was made through fusion of remote sensing products, reanalysis dataset and in-situ observation data, obtained from National Tibetan Plateau Data Center (He et al., 2020; Yang et al., 2010a, 2010b). Annual PO and GDP data by province were downloaded from the website of the China National Bureau of Statistics (http://www.stats.gov.cn/tjsj/ndsj/).

We note that the AL and WD data for lakes in this study are constant values during the time due to the lack of time-series data, while the other parameters change throughout the time domain. The summer (i.e., from June to September) mean values for the long-term SA, NDVI, AT, PR, and WS data were produced for each year from 2000 to 2017 to be consistent with the periods of derived water clarity data. Annual PO and GDP data by province were used for the time series analysis. Spatially, the local NDVI, AT, PR, and WS data for each lake were computed as the average value of the NDVI, AT, PR, and WS data in the watershed in which the lake is located. The watershed boundaries are specified by China's Third-level Watershed, obtained from the Resource and Environment Data Cloud Platform (http://www.resdc.cn/data.aspx? DATAID = 278). The local GDP and PO data for each lake corresponded to the GDP and PO data for the province in which the lake is located.

3. Estimation of Z_{SD} from MODIS

3.1. MODIS preprocessing

Fig. 2 shows a flowchart of the MODIS preprocessing to estimate Z_{SD}. Prior to the chromaticity parameter calculation (i.e., the FUI and α), two essential steps in the preprocessing were followed, i.e., the

remote sensing reflectance correction to derive R_{rs} from MODIS and water segmentation to extract water areas from MODIS.

For the remote sensing reflectance correction, a pixel-based correction method (Wang et al., 2016; Wang et al., 2018) was used. This method subtracts the minimum value of the near infrared and shortwave infrared bands from reflectance of each band. The pixel-based correction method reduces residual noise in the MOD09A1 data, including the residual aerosol effect, skylight reflection, and sun glint, and converts the MOD09A1 surface reflectance to R_{rs}. It has also been demonstrated that this method works well for the three visible bands over a wide range of inland waters with R_{rs} retrieval uncertainties of approximately 30% (Wang et al., 2016).

Water areas were first automatically segmented from MOD09A1 data using the MODIS 6th band (centered at 1640 nm) following the water extraction scheme proposed in Wang et al., 2018. To avoid the severe land adjacency effect, a 500 m buffer inward of the water boundary was removed for each water body. Optically shallow waters were removed to avoid the effect of the water bottom using the method described in Wang et al., 2018. Image pixels covered by clouds, ice, snow, and other noise were detected using the MOD09A1 QA data and removed from the analysis. At the same time, obvious aquatic vegetation areas were identified and removed. Algae bloom areas, identified using the Floating Algae Index (FAI) method, with a threshold of 0.004 (Duan et al., 2015; Hu, 2009), were removed from the water areas.

FUI and α are two closely related water chromaticity parameters that can be derived from MODIS visible bands (Wang et al., 2015; Wang et al., 2018). While α increases continuously from blue to yellowish-brown color, FUI divides these colors into 21 classes. There are five main steps in FUI and α calculation using the MODIS R_{rs} following the method and scheme described in Wang et al. (2015) and Wang et al. (2018):

- Computation of the CIE tristimulus values (i.e., X, Y, and Z) (C.I.E., 1932) from the MOD09 R_{rs} in the visible bands using the RGB conversion method,
- Calculation of the CIE chromaticity coordinates (x, y) by normalizing X, Y, and Z to between 0 and 1,
- Calculation of α from the chromaticity coordinates (x, y) where α increases from 0° to 360° as water color changes from blue to yellowish-brown color (Wang et al., 2018),
- A delta correction was made for α to eliminate the color difference caused by the MODIS band setting following the method detailed in Wang et al., 2018, and

(5) The FUI for each pixel in MOD09 was calculated from α based on the 21-class FUI lookup table (Table 2). We note that α in this study remains consistent with that reported in Wang et al. (2018), i.e., increasing with increases in FUI.

Table 2
Chromaticity coordinates (sourced from Novoa et al., 2013) and corresponding hue angle α look-up table for FUI indices from 1 to 21.

FUI	x	y	α	FUI	x	y	α
1	0.1914	0.1669	40.4670	12	0.4024	0.4811	205.0622
2	0.1990	0.1999	45.1963	13	0.4162	0.4737	210.5766
3	0.2100	0.2399	52.8527	14	0.4313	0.4655	216.5569
4	0.2265	0.2883	67.1695	15	0.4457	0.4576	222.1153
5	0.2459	0.3353	91.2980	16	0.4606	0.4494	227.6293
6	0.2662	0.3762	122.5852	17	0.4753	0.4410	232.8302
7	0.2908	0.4115	151.4792	18	0.4887	0.4328	237.3523
8	0.3154	0.4400	170.4629	19	0.5033	0.4246	241.7592
9	0.3367	0.4617	181.4983	20	0.5155	0.4161	245.5513
10	0.3633	0.4764	191.8352	21	0.5283	0.4083	248.9529
11	0.3862	0.4866	199.0383				

3.2. Z_{SD} model development

Previous studies (Garaba et al., 2015; Li et al., 2016; Pitarch et al., 2019) have shown that bluer and clearer waters are characterized by a lower FUI index. In contrast, more turbid and yellow waters result in a higher FUI index. In this study, we analyzed the relationship between Z_{SD} and FUI based on both the simulated and in-situ measured match-up datasets. We then developed an empirical model for Z_{SD} using the 183 measured match-up pairs. It indicated that Z_{SD} and FUI are characterized by significant negative exponential correlations in both the simulated and the measured match-up datasets (R^2 = 0.95 and 0.93, respectively, in Figs. 3 and 4), confirming the strong relationship between Z_{SD} and FUI (Li et al., 2016; Pitarch et al., 2019). We note that the empirical parameters in the Z_{SD} fitting model are different between the simulated and measured datasets (as shown in Figs. 3, 4(a), and 4(b)). This is because (1) the simulated dataset covers a larger FUI range from 1 to 21 while the measured data set only includes FUI from 3 to 17 due to the fact that water color in large lakes is normally unable to cover extreme blue or brown colors and (2) the simulated dataset was generated based on bio-optical models mainly for oceanic waters (IOCCG, 2006), which will not represent all the complex situations in inland waters. However, the OACs and underwater light field in inland waters over such a large area can vary in a wide range, such that the relationship between Z_{SD} and FUI is a little loose for the measured dataset. The effect of one specific or more OACs in water on the relationship between Z_{SD} and FUI will be discussed in Section 5.1.

However, we found that when the FUI value is low (i.e., FUI < 8), there is a scattering in the relationships for both datasets compared with strong relationships when FUI ≥ 8. In other words, one FUI value may correspond to a Z_{SD} range rather than one value for relatively clear waters when FUI < 8. To manage the shortcomings of the dispersive FUI in clear waters, we also analyzed the relationships between α and Z_{SD}. Both Figs. 3 and 4 show that the correlations between α and Z_{SD} were better than that between FUI and Z_{SD} when FUI < 8. When FUI ≥ 8, the separating ability between α and Z_{SD} was compressed compared with the separation between FUI and Z_{SD}. Hence, by considering the actual situation in lakes, a hybrid Z_{SD} estimation model was developed using FUI and α based on the measured match-up dataset:

$$\begin{cases} \text{FUI} < 8: Z_{SD} = 3415.63 * \alpha^{-1.49} \\ \text{FUI} \geq 8: Z_{SD} = 284.70 * \text{FUI}^{-2.67} \end{cases} \quad (1)$$

Here, the empirical parameters in the model for FUI < 8 were generated using measured data with α < 195° (i.e., FUI < 11) to ensure a smooth transition between the two ranges. We note that in the measured dataset, the sensitivity of alpha to Z_{SD} is a little bit low when α < 195° (Fig. 4 (c)) because the samplings in clear lakes with α < 195° were limited due to the poor measurement conditions in Tibetian Plateau. And we expect when the Z_{SD} is very large, the uncertainties in the measured Z_{SD} data could be a little higher because the measurement may be impacted by a tilted scale rope or the observer's sight.

3.3. MODIS Z_{SD} model validation

The performance of the FUI and α-based model was tested with the independent in-situ measured Z_{SD} dataset. The MAD and MRD, which describe model errors, are defined as follows:

$$\text{MAD} = \frac{\sum |X_i - x_i|}{N} \quad (2)$$

$$\text{MRD} = \frac{\sum \frac{|X_i - x_i|}{x_i}}{N} \quad (3)$$

where X_i and x_i are the model estimated value and in-situ measured value, respectively, and N is the number of match-up pairs.

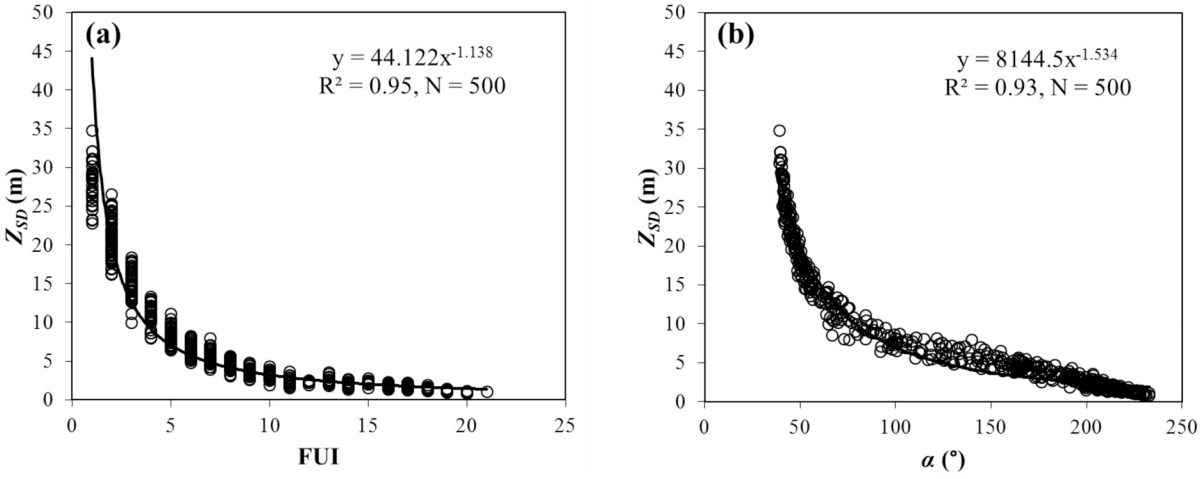

Fig. 3. Scatterplots of (a) Z_{SD} and FUI and (b) Z_{SD} and α based on the Hydrolight simulated dataset.

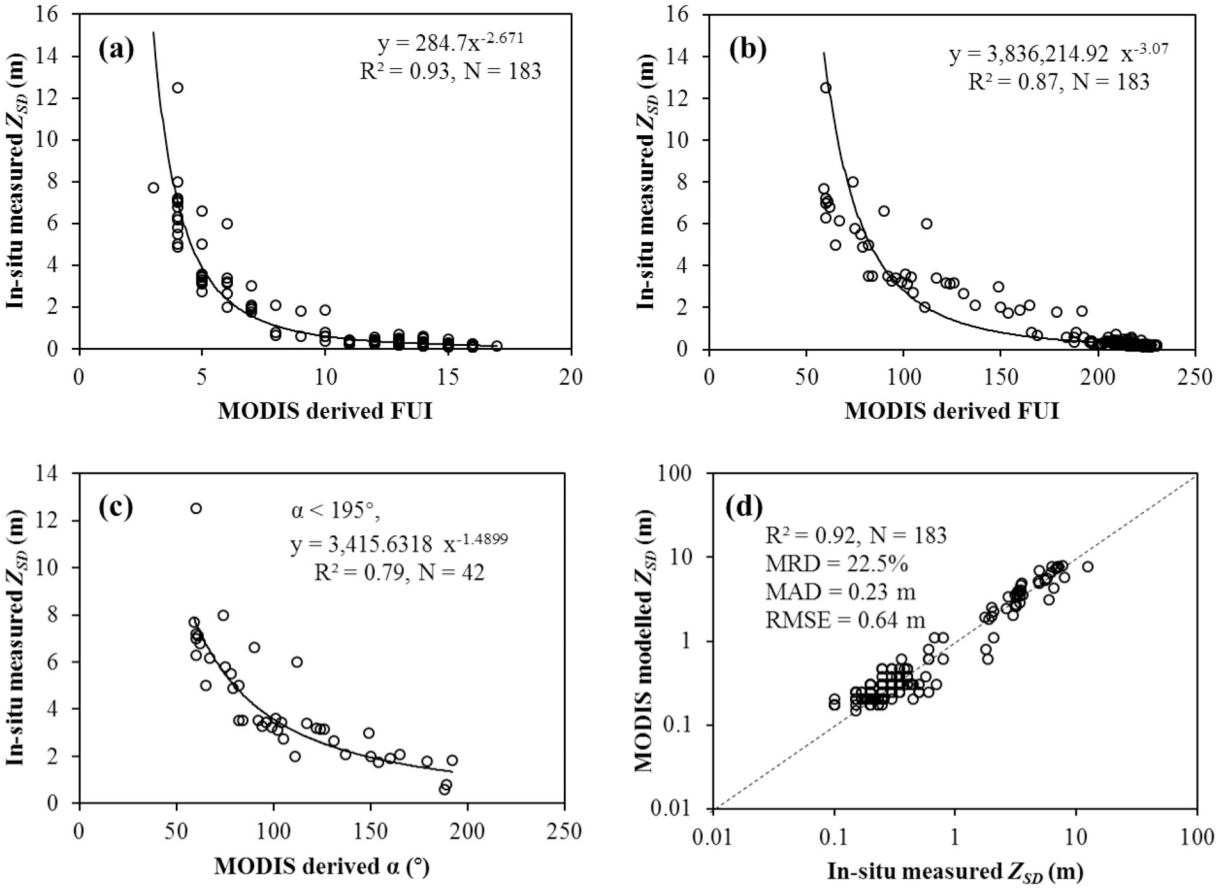

Fig. 4. Scatterplots of the (a) in-situ measured Z_{SD} and MODIS derived FUI, (b) in-situ measured Z_{SD} and α, (c) in-situ measured Z_{SD} and MODIS α when α < 195°, and (d) in-situ measured Z_{SD} and the MODIS estimated value with FUI and α based on the match-up pairs. MRD and MAD are defined in Section 3.3.

It showed that the MODIS model derived Z_{SD} agreed well with the in-situ measured Z_{SD} for the 17 validation lakes with Z_{SD} ranging from 0.2 to 13.1 m (Fig. 5). The MRD value was only 27.4% and the MAD value was 0.37 m, which were generally consistent with the performance when the model was developed. Fig. 6 showed the MRD of the FUI and α-based model with different Z_{SD} ranges based on the validation dataset. There was no significant difference in the MRD of this model for different Z_{SD} ranges, with median values of MRD mainly below 40%. The results indicate that MODIS derived FUI and α can be used with satisfactory performance to retrieve the Z_{SD} for the validation dataset from different types of inland waters, i.e., ranging from clear oligotrophic lakes to extremely turbid and eutrophic waters. Thus, this FUI and α-based model can be used to map the long-term Z_{SD} distribution patterns for inland waters in China from MOD09A1 image data collected from 2000 to 2017. This allows the study of the spatial and temporal changes in Z_{SD} for Chinese inland waters.

3.4. Calculation of spatial and temporal statistics

Water bodies larger than 25 km^2 in surface area were selected as the

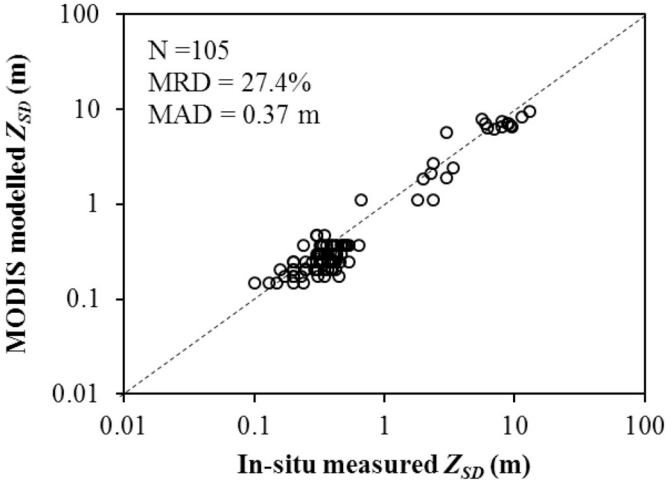

Fig. 5. A scatterplot of the in-situ measured Z_{SD} and the synchronous MOD09GA derived Z_{SD} based on the independent validation dataset.

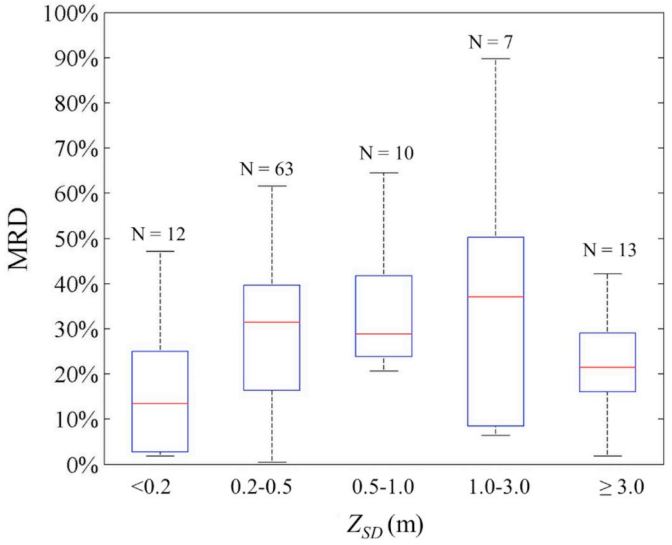

Fig. 6. A boxplot showing the MRD (mean relative difference) values of the Z_{SD} model in different Z_{SD} ranges.

target water bodies in this study, where the Z_{SD} model was applied to the high-quality MODIS 8-day surface reflectance data to obtain the water clarity in the summer months (i.e., from June to September). The four summer months were selected to avoid the influence of ice/snow cover on the lakes in north and west China. The mean summer Z_{SD} for each year during the 18 year period and the mean 18-year climatological summer Z_{SD} for every water body were estimated. When calculating the mean summer Z_{SD} for each water body, if the water area in one image was less than 30% of the normal water mask, this water area was not used to calculate the average summer result due to lack of spatial representation. The normal water mask for each water body was obtained by overlaying the water masks segmented from MODIS images during the 18 years. If there were less than 3 valid images for one water body during the summer in one year, the average summer Z_{SD} was not calculated for this water body in this year. Moreover, broken waters that were separated into parts by MODIS tiles, clouds, and image noise were merged using the normal water mask to calculate the mean summer value. In the long-term trend analysis, only water that had at least 12 years of valid mean summer Z_{SD} values from 2000 to 2017 were included in the analysis for a reliable time-series analysis. With the criteria stated above, 65 lakes were removed from 218 extracted waters, and the remaining 153 waters were studied further. For the studied water bodies, we conducted linear regression against time over the mean summer Z_{SD} values for each water body, where the associated slope was obtained as the change in the annual Z_{SD} rate from 2000 to 2017. To determine if the increase or decrease was significant, the *p*-values associated with the linear regression were also calculated, where statistically significant trends had p-values of less than 0.05.

4. Spatial and temporal patterns of water clarity across China

4.1. Spatial patterns of lake clarity across China

The climatological mean summer Z_{SD} values between 2000 and 2017 for the 153 large lakes were produced following the procedures described in Section 3 using MOD09A1 reflectance data as the input. Mean summer Z_{SD} values in these aquatic systems exhibited a wide range (0.1 to 10 m), showing a large diversity in Chinese lakes. The Z_{SD} values of large lakes exhibited a distinct geographical pattern of "high west and low east" in China (Figs. 7(a) and 7(c)). Most lakes with high Z_{SD} values (i.e., > 5.0 m) are located in the QTR while most lakes with low Z_{SD} values (i.e., < 0.5 m) are located in the EPR and NER. The Z_{SD} values also depicted a general latitudinal pattern of "high south and low north" (Fig. 7(b)). However, water clarity significantly varied across the same latitude.

The study area was also divided into the east China and west China using the Heihe-Tengchong Line (H-T Line) geo-democratic demarcation line (Hu, 1990; Ge and Feng, 2008). Here the east China includes EPR, YGR and NER, and the west China includes QTR and MXR. The Z_{SD} values at 69% of the lakes located in the west were greater than 2 m while 61% of the lakes located in the east were lower than 0.5 m (Fig. 7(d)). For the five geographic lake regions, lakes in the QTR showed high levels of Z_{SD}, with an average value of 3.9 m, whereas lakes in the EPR exhibited low Z_{SD}, with an average value of 0.6 m. Only two reservoirs (i.e., the Danjiangkou and Xin'anjiang Reservoirs) appeared to be clearer than 1 m of Z_{SD}. All three studied lakes in the NER had the lowest level of Z_{SD}, with an average value of 0.2 m while lakes in the MXR and YGR showed diverse Z_{SD} values (Figs. 7(a) and (e)).

Fig. 8 shows a map of climatological summer Z_{SD} for several typical large lakes. The water clarity spatial patterns in these lakes were manifested in the climatological maps. For example, for the majority of the lakes, the Z_{SD} values were high in the central part of the lake and low near the shoreline. Estuary regions in Qinghai Lake and Namco Lake can be identified based on low values in the maps. In Taihu Lake, it was found a clarity gradient with low values on the western side and higher values on the eastern side. These results are consistent with previous studies (Feng et al., 2019b; Shi et al., 2018).

4.2. Temporal patterns of lake clarity across China between 2000 and 2017

The mean summer Z_{SD} of the 153 studied large lakes from 2000 to 2017 was derived using MODIS data following the procedures described in Section 3 and shown in Fig. 9, where the lakes in each lake region were arranged with annual change rate from low to high. The annual change rate of the mean summer Z_{SD} between 2000 and 2017 for the studied lakes was mapped in Fig. 10, where lakes with statistically significant increases or decreases were marked. The average annual change rate of all studied lakes was 3.3 cm/yr, 4.1 cm/yr for lakes located west of the H-T Line, and only 0.2 cm/yr for lakes located east of the H-T Line. The results also revealed that 38.6% (59 in total) of all the lakes experienced a significant increase in water clarity during the last 18 years while only 8.5% (13 in total) of the lakes had a significant decreasing pattern in water clarity. Nevertheless, only 7 of the 72 lakes with significant annual changes in their Z_{SD} were east of the H-T Line. Water clarity in 12.9% of the lakes located east of the H-T line had a significantly increasing trend while 9.7% showed a significantly

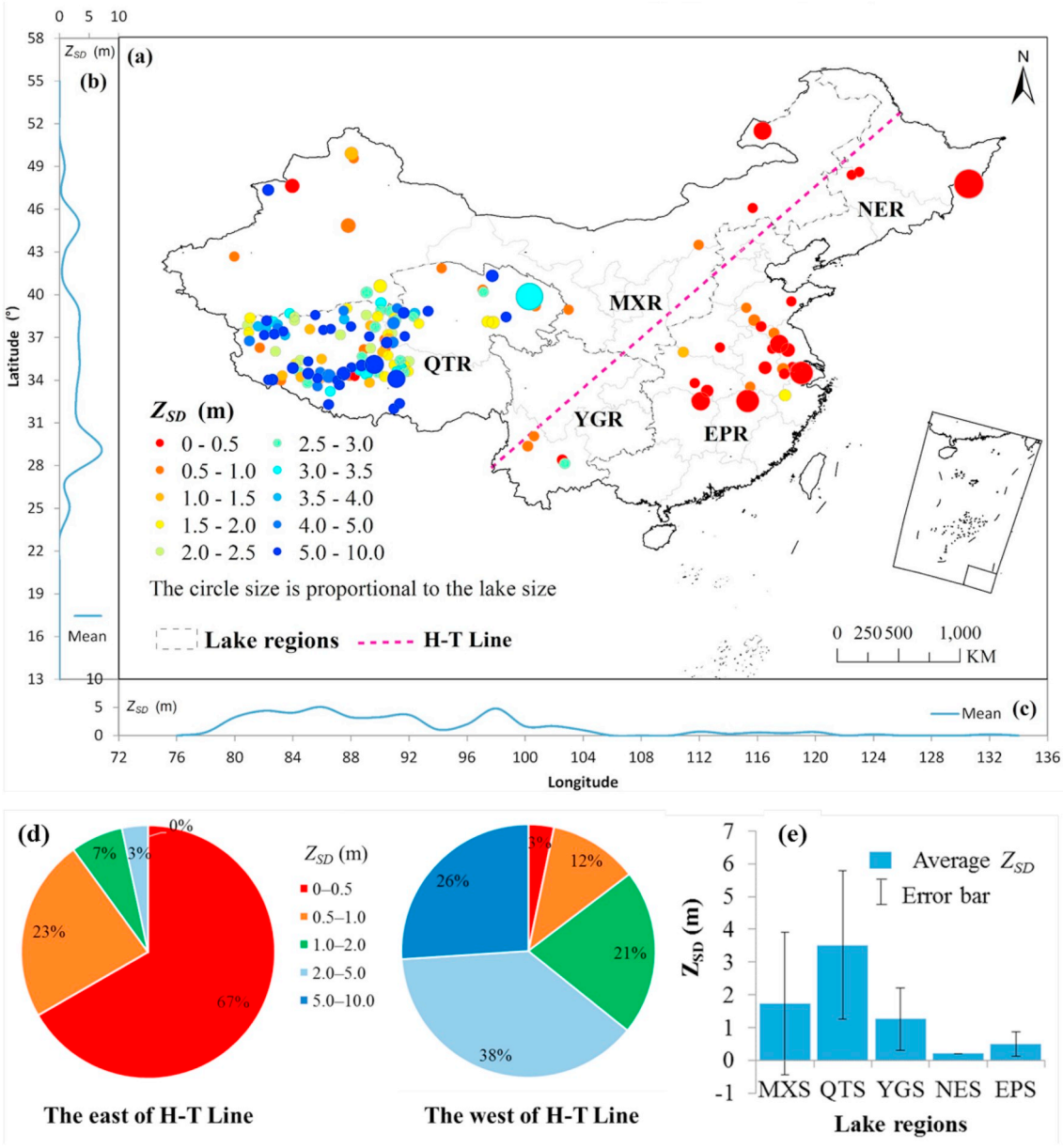

Fig. 7. (a) The climatological mean summer Z_{SD} from 2000 to 2017 for large lakes in China, (b) the climatological Z_{SD} with 2° latitude averages of large lakes, and (c) the climatological Z_{SD} with 2° longitude averages of large lakes. (d) pie charts of the mean summer Z_{SD} for large lakes in east and west China divided by the H-T Line (Heihe-Tengchong Line), (e) the average Z_{SD} and standard deviation of lakes' Z_{SD} (shown as error bars) in the five lake regions.

decreasing trend (shown in Supplementary Material as Fig. S1). To the west of H-T Line, the percentages of lakes that had significant increasing or decreasing trends were 44.7% and 8.2%, respectively (shown in Supplementary Material as Fig. S1). This indicated that there was a weak changing trend in water clarity for large lakes east of the H-T Line while large lakes west of the H-T Line experienced a dramatic increase in water clarity from 2000 to 2017.

For the five geographic lake regions, the mean summer Z_{SD} values of the lakes increased drastically in the QTR during the analysis period (shown in Supplementary Material as Fig. S2). In the QTR, a number of large lakes, such as Namoco, Zhari Namco, and Geruco, experienced a significant increase (> 10 cm/yr) in water clarity. However, Lake Qinghai and Lake Silingco, two well-known large lakes in the QTR, had significant decreases in their water clarity, with an annual decreasing rate of approximately – 10 cm/yr. Increases in the mean summer Z_{SD} were relative minor in the EPR, NER, and MXR. In the EPR, Lake Shijiu and Lake Nanhu exhibited significant decreases in water clarity, with an annual decreasing rate of approximately – 2 cm/yr, while Danjiangkou Reservoir, Suyahu Reservoir, and Lake Nvshanhu were characterized by significant increases in water clarity, with annual increasing rates of 5.4, 1.2, and 0.6 cm/yr, respectively. In the NER, the Nanyin Reservoir showed a significant increase in water clarity with an annual change rate of 0.7 cm/yr. In the MXR, Lake Sayram was characterized by a significant increase in water clarity with an annual change rate of 6.0 cm/yr while Lake Ebinur, Lake Daihai, and Lake Hulun exhibited significant decreases with annual decreasing rates of – 1.4, − 0.6, and – 0.4 cm/yr, respectively. The YGR, however, was the only region where the average lake Z_{SD} experienced a decrease from 2000 to 2017 (shown in Supplementary as Fig. S2), especially Lake Chenghai, which showed a significant decrease in water clarity with an annual decrease rate of – 3.7 cm/yr. Previous studies have reported similar results for lake clarity trends in the EPR and YGR (Feng et al., 2019a; Zhou et al., 2019).

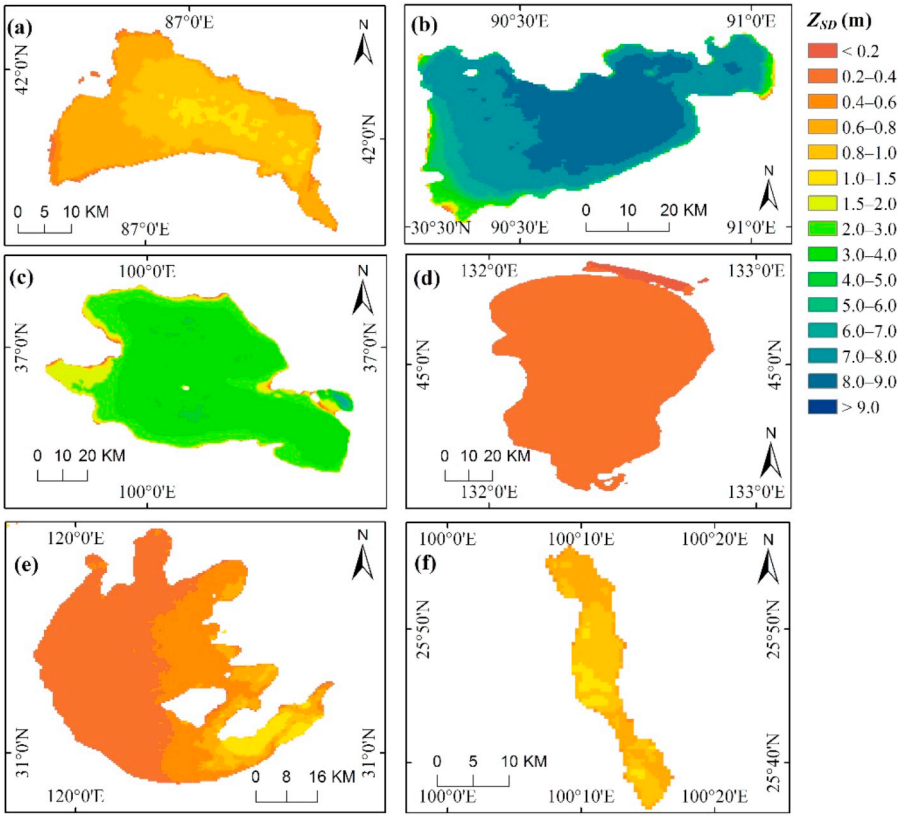

Fig. 8. The climatological mean summer Z_{SD} in several typical lakes in China between 2000 and 2017. (a) Bositeng Lake, (b) Namco Lake, (c) Qinghai Lake, (d) Xingkai Lake, (e) Taihu Lake, and (f) Erhai Lake. The locations of these six lakes are shown in Fig. 1.

5. Discussion

5.1. Why use water color parameters to estimate lake clarity?

Good correlations between water color and water clarity have been observed in extensive measurements by groups over a wide range of inland and oceanic waters (Wang et al., 2015; Li et al., 2016; Garaba et al., 2015; Pitarch et al., 2019). Like water clarity, water color is also an indicator of the overall water quality, which will change with the overall amount of dissolved and suspended matter in water column (Wang et al., 2015; Pitarch et al., 2019). Based on the IOCCG simulated dataset (IOCCG, 2006), the relationship between water color and the OACs in water in terms of absorption coefficient of phytoplankton pigment (a_{ph}), absorption coefficient of CDOM (a_g), absorption coefficient of detritus and minerals (a_d) was shown in Fig. 11. Although the changing slope is a little bit different for a_{ph}, a_g, a_d, as a whole no matter which component dominated, the water color will change with total absorption coefficient of the water column (a_{total}) in a basically consistent exponent way (Fig. 11 (d)). More importantly, the changes of a specific component proportion in water would not significantly influence the relationship between Z_{SD} and water color, as illustrated in Fig. 12, as long as the water color is not driven by one constituent. The

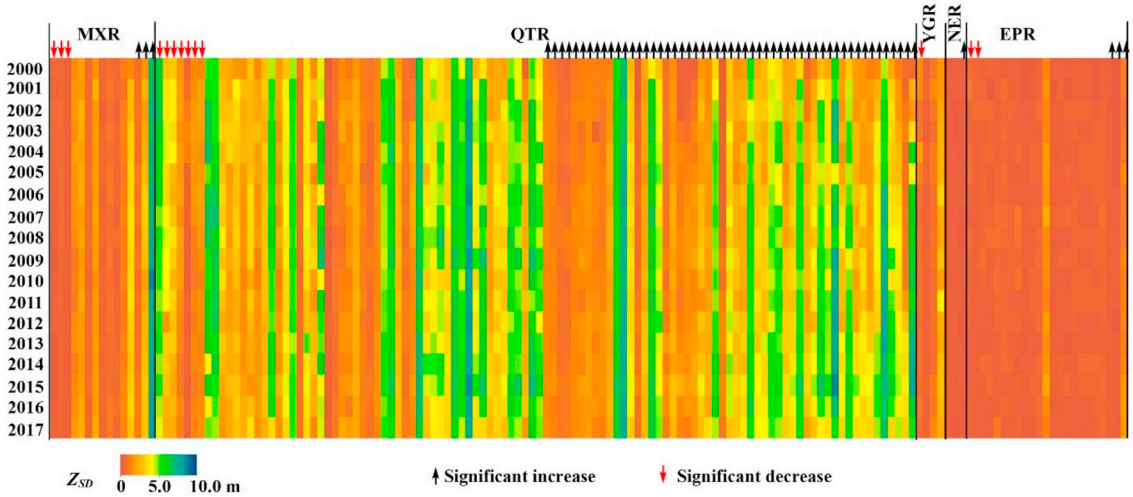

Fig. 9. A heat map showing the mean summer Z_{SD} from 2000 to 2017 for large inland waters across the five lake regions in China. The lakes in each lake region were arranged with annual change rate from small to large and lakes with statistically significant increases or decreases were marked.

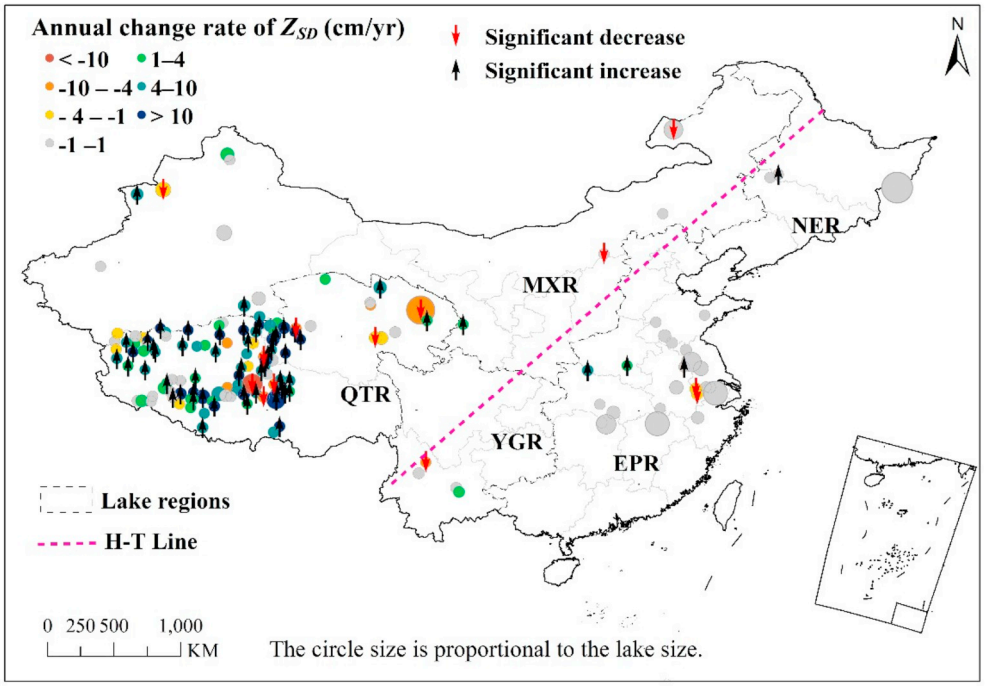

Fig. 10. The annual change rate of mean summer Z_{SD} for large inland waters from 2000 to 2017. Lakes with significant ($p < .05$) increase and decrease in summer Z_{SD} were marked.

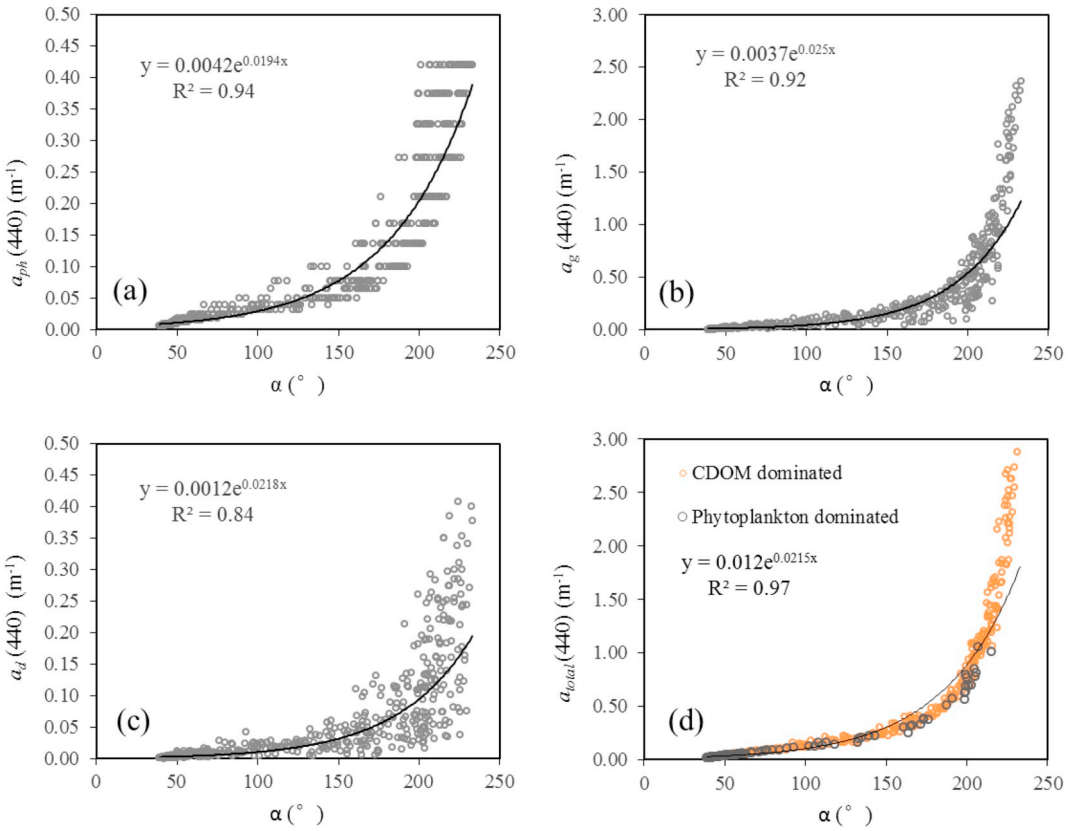

Fig. 11. Scatterplots of hue angle α versus (a) absorption coefficient of phytoplankton $a_{ph}(440)$, (b) absorption coefficient of CDOM $a_g(440)$, (c) absorption coefficient of suspended matter $a_d(440)$, (d) total absorption coefficient of water column $a_{total}(440)$. CDOM- and phytoplankton-dominated water points were marked with different colors in Fig. 11 (d).

partial correlation between hue angle α and Z_{SD} through controlling the effect of a_{ph}, a_g, a_d, together with backscattering coefficients bb_d (backscattering coefficient of detritus and minerals) and bb_{ch} (backscattering coefficient of Chl-a) further confirmed the robust and internal relationship between α and Z_{SD}, as the significant correlation between α and Z_{SD} was barely affected by the absorption or

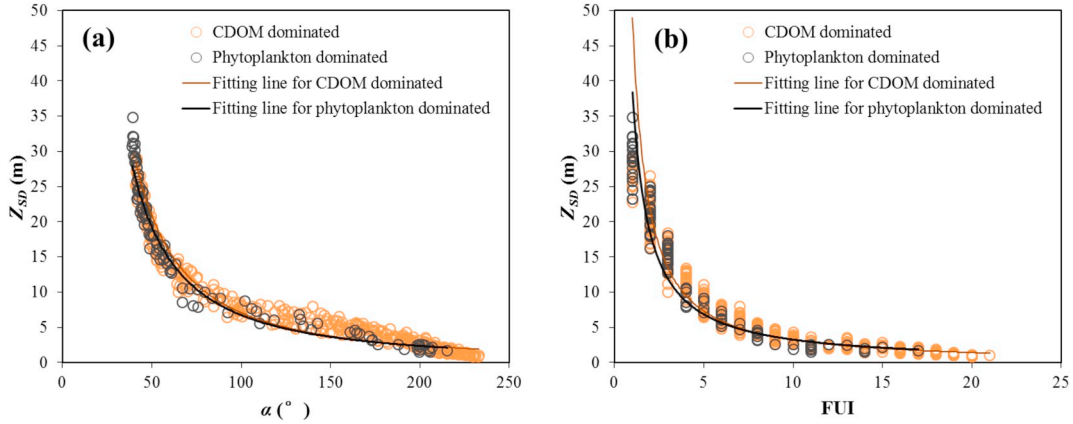

Fig. 12. Scatterplots of Z_{SD} versus (a) hue angle α, (b) FUI based on the simulated dataset (IOCCG, 2006). CDOM- and phytoplankton-dominated water points were marked with different colors.

Table 3
Correlation and partial correlation coefficient between hue angle α and Z_{SD} while controlling for one or more color components in water, in terms of absorption coefficient of phytoplankton pigment (a_{ph}), absorption coefficient of CDOM (a_g), absorption coefficient of detritus and minerals (a_d), backscattering coefficient of detritus and minerals (bb_d) and backscattering coefficient of Chl-a (bb_{ch}), based on the IOCCG simulated dataset.

Control variable		Z_{SD}
–	α	−0.90*
a_{ph}(440)	α	−0.82*
a_g(440)	α	−0.85*
a_d(440)	α	−0.86*
bb_d(600)	α	−0.85*
bb_{ch}(600)	α	−0.85*
a_{ph}(440) & a_g(440) & a_d(440)& bb_d(600) & bb_{ch}(600)	α	−0.82*

Note: * denotes significant correlation with $p < .01$.

backscattering of the OACs with the correlation coefficient decreased from 0.90 to 0.85 (Table 3). As the relationship is still 'empirical' at this stage, further analytical efforts and explanations are expected in future research. In fact, the new Z_{SD} analytical model indicates that Z_{SD} is determined by K_d at the transparent window (K_d^{tr}), and the transparent window is actually determined by the perceived water color (Lee et al., 2015), which implies the physical relation between Z_{SD} and water chromaticity color. But we note that, in Fig. 11, the fitting effect between α and the absorption coefficients is not very good when the absorption coefficient is very high. It is probably due to the 'end-point' of natural water color which has been reported in Wang et al., 2015 that when one or more of the OACs are extremely high in water, the water color hue angle will tend to be saturated around 235°. This would potentially lead to an overestimation of Z_{SD} in very turbid waters which will be further discussed in Section 5.2.

To further answer the question of why use chromaticity parameters to estimate lake clarity, we compared the Z_{SD} model developed in this paper with other published Z_{SD} empirical models based on the in-situ R_{rs} and Z_{SD} dataset. The published Z_{SD} empirical models included empirical algorithms based on band-ratio (Duan et al., 2009; Kratzer et al., 2008; Ren et al., 2018), single-band (Binding et al., 2015; Shi et al., 2018) and band combinations (Olmanson et al., 2016; Olmanson et al., 2008). The models were tuned and optimized to fit the in-situ dataset. This in-situ R_{rs} and Z_{SD} dataset was not used to develop the model in this paper because it contains very few R_{rs} data from relative clear lakes (only 15 samplings in Qinghai Lake), which seems to be lack of the representativeness in clear lakes. It shows that the FUI and α-based algorithm proposed in this study outperformed other empirical models with MRD of 25.8% and MAD of 0.08 m (Fig. 13). Model based on FUI itself also achieved good performance with the MRD of 26.5% and MAD of 0.11 m, but slightly worse than the hybrid model, which confirmed the respective suitable range of FUI and α for Z_{SD} estimation. Although the parameters in the Z_{SD} model (as shown in Fig. 13 (a)) are a little different with that developed in Section 3.2 after optimizing with the in-situ R_{rs} and Z_{SD} dataset, the model developed in Section 3.2 can also produce better results for this dataset than other models with MRD of 26.1% and MAD of 0.09 m. In the rest models, the Red-to-Green band ratio models optimized from Duan et al. (2009) and Ren et al. (2018) generally had good performances with MRD of 28%–29% and MAD of 0.10–0.13 m. Besides, there were general over-estimations when $Z_{SD} < 0.1$ m, which means that when the water is extremely turbid, the sensitivity of water color, single band, band ratio, etc. to Z_{SD} will decrease. The comparison results indicated that water chromaticity parameters (FUI and α) can better estimate Z_{SD} in a wide range than other empirical models. Moreover, FUI and α have high tolerance to the atmospheric perturbations and observation conditions (Wang et al., 2018), which further promote the use of FUI and α for Z_{SD} estimation over various types of inland waters across large regions where accurate atmospheric correction is still very difficult to tackle at present.

5.2. Algorithm uncertainties

Over recent decades, there have been a growing number of radiometric measurements for water quality variables via satellites. Remote sensing of water quality variables is based on the concept that variations in water constituents can change the spectrum of water color (IOCCG, 2018). Due to the special characteristics of inland waters, two main issues must be addressed when deriving water quality at large scales using remote sensing technology: adaptability of the algorithm to various optical water types (OWTs) and atmospheric correction.

In this study, good relationships have been found between Z_{SD} and FUI and α over a wide range of Z_{SD} based on three types of datasets: simulated dataset, in-situ dataset, and MODIS match-up dataset. In Section 5.1, the intrinsic relationship between Z_{SD} and FUI and α have been discussed and the advantages of FUI and α-based Z_{SD} model have been shown through comparing with other published models. These together demonstrate the generalization capacities of this FUI and α-based algorithm over lakes in a variety of conditions and optical types. Like other OWT-based algorithms (Neil et al., 2019), it can achieve a better overall accuracy compared with algorithms developed for specific waters.

The estimation model was merged by the FUI and α because the FUI contains relatively coarse colors when it is smaller than 8 and α is a good alternative in this range to describe variations in the water clarity, which have been also observed in ocean waters (Pitarch et al., 2019). Our results also showed that using FUI or α alone for Z_{SD} estimation can also achieve good performances, but not as robust as the hybrid model,

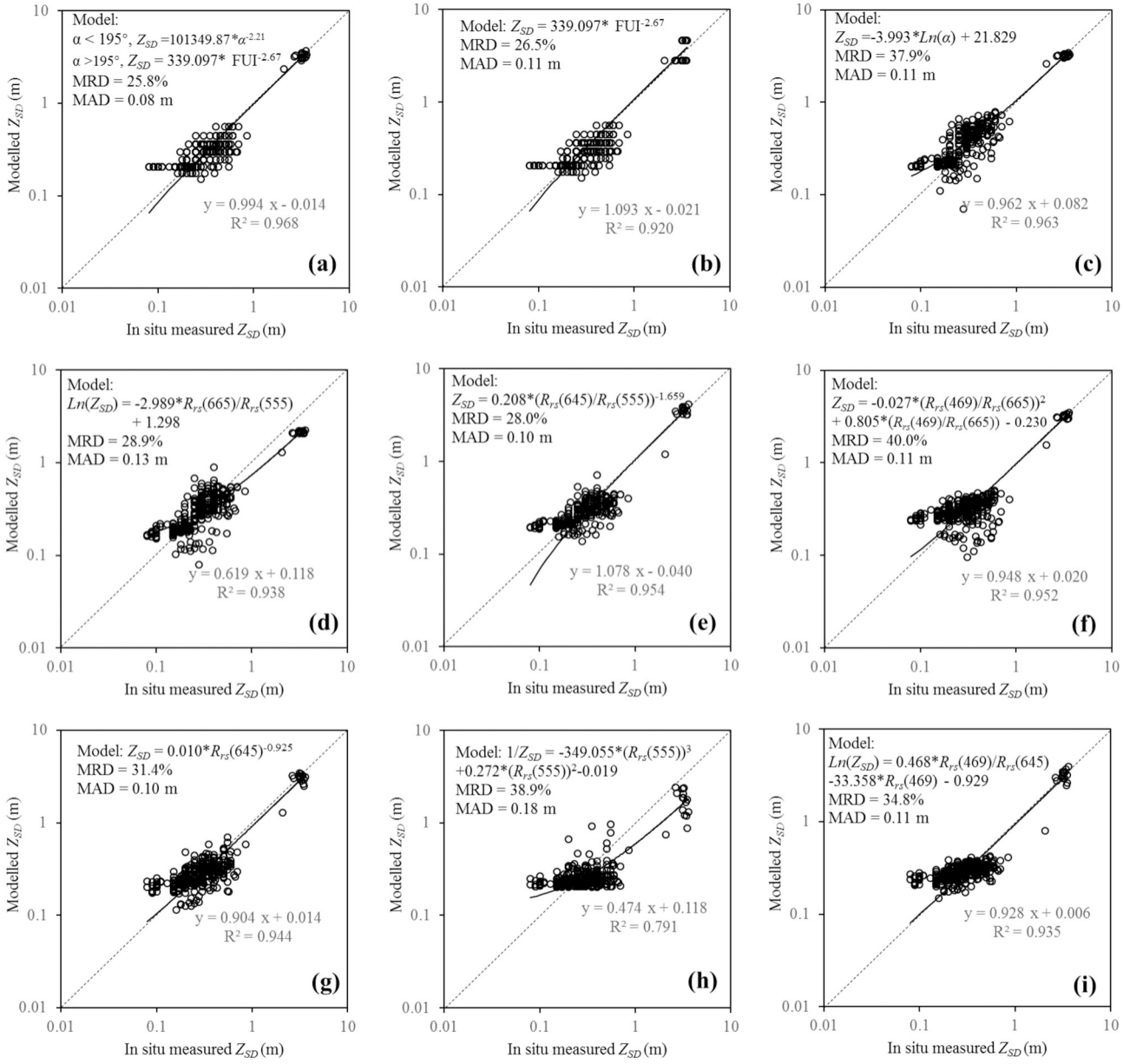

Fig. 13. Model performance comparison of FUI and α-based algorithm and other published Z_{SD} estimation algorithms optimized and calibrated by the in-situ R_{rs} and Z_{SD} dataset. (a) Model performance of FUI and α-based algorithm; (b) Model performance of FUI-based algorithm; (c) Model performance of α-based algorithm; (d) and (e) Model performances of Red-to-Green band-ratio algorithms optimized from Duan et al. (2009) and Ren et al. (2018) respectively; (f) Model performance of Blue-to-Red band-ratio algorithm optimized from Kratzer et al. (2008); (g) and (h) Model performances of single-band algorithm optimized from Shi et al. (2018) and Binding et al. (2015) respectively; (i) Model performance of band-combination algorithm optimized from Olmanson et al. (2008, 2016). (For interpretation of the references to color in this figure legend, the reader is referred to the web version of this article.)

which confirmed the respective suitable range of FUI and α in estimating Z_{SD}. That is to say, when water color is green or yellow, a change of FUI can better represent the change of water clarity, but when water color is blue, a change of hue angle α is better. Nevertheless, we expect that there are some uncertainties when applying the model to such a wide range of datasets from various types of lakes. We observed that there is a slight overestimation of the estimated Z_{SD} when Z_{SD} is very small (< 0.1 m) for both the in-situ dataset and validation dataset (as shown in Fig. 4 (d), Fig. 5 and Fig. 13). This is likely due to the "end-point" (~235°) of hue angle in natural waters where one or more of the components reach extreme high values, which have been reported in previous studies (Wang et al., 2015). Under these extreme conditions, the Z_{SD} will be less than 0.1 m and water color is unlikely to further change with Z_{SD}.

Besides, we note that the FUI and α can only describe the dominant color wavelength but they lose information on color purity. A recent study has shown that color purity is also sensitive to water quality (Shen et al., 2019), which may further support water clarity retrieval in future studies.

The MODIS surface reflectance product (MOD09) was selected as the satellite data source in this study which have been proven to be applicable to water quality mapping in many inland waters (Hou et al., 2017; Li et al., 2016). A correction method for MOD09 proposed in Wang et al. (2016) was used to reduce the remaining noises and derive R_{rs} by subtracting a minimum value in near-infrared (NIR) and shortwave infrared (SWIR) bands. The validity of the subtraction logic was also demonstrated in other studies to derive R_{rs} from Rayleigh-corrected MODIS reflectance (Feng et al., 2018b). In addition, we found

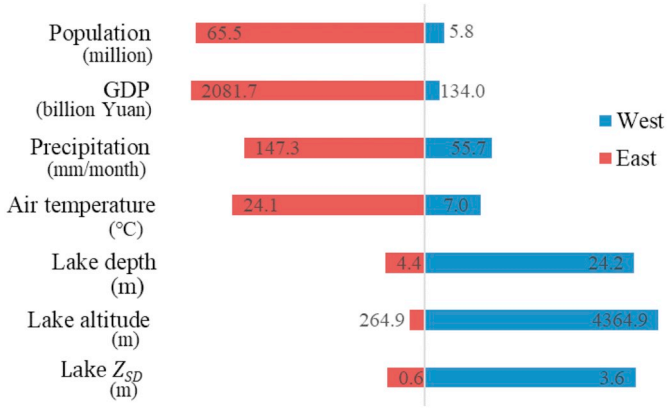

Fig. 14. A bar chart of the average Z_{SD} and average value of local environmental factors for lakes located in west and east China, separated by the H-T Line.

that the data quality of daily MOD09 data (MOD09GA) was not as good as that of the 8-day composite MOD09 data (MOD09A1), as more invalid negative values were occurred in MOD09GA, especially at pixels near cloud covers and at clear lakes in west China. It is because the MOD09A1 data is selected as the best possible reflectance observation of MOD09GA data during the 8-day period at the pixel level with the criteria including cloud and solar zenith (Vermote, 2015). That is why we use the 8-day MOD09A1 data other than 1-day MOD09GA data for the long-term water clarity observation and analysis in this study. But in order to narrow the match-up window in the model development, we still use the daily MOD09GA data to build the match-ups after removing pixels containing clouds and other noises. The consistency between the 1-day MOD09GA and 8-day MOD09A1 data in the long-term Z_{SD} estimation was demonstrated and shown in Supplementary as Fig. S3. Another reason for using the MOD09 data is that it is a long-term time series from 2000 to the present, which is not the case for certain new sensors. With the improved radiometric calibration of all MODIS Terra products, which account for the sensor degradation, the long term change analyses based on MODIS Terra have been demonstrated in a number of studies (Hou et al., 2017; Wu et al., 2008). But we also note that the 8-day composite MOD09A1 data would be not suitable for studies which intend to explore the daily dynamics of lakes considering its coarse temporal resolution. New satellite sensors with finer temporal resolution and spatial resolution may bring more advantages to water quality monitoring and enable more detailed monitoring over lakes where the changes are more rapid and local compared to open oceans. More importantly, it has been proven in many studies that the derivation of the FUI and α from MODIS or other sensors is very robust (an accuracy of ~90%) (Lehmann et al., 2018; Van der Woerd and Wernand, 2018; Wang et al., 2015; Wang et al., 2018), which can eliminate errors in the remote sensing reflectance product, taking advantage of the normalization process in calculation (Wang et al., 2018). The FUI and α retrieval algorithm has a high tolerance to the spectral resolution of satellite images (Van der Woerd and Wernand, 2018). Hence, the broad visible bands of MODIS can be used to estimate Z_{SD}. This advantage of the FUI and α can also bridge the gap between low spectral sensors and the new high spectral sensors for Z_{SD} estimation (Van der Woerd and Wernand, 2018). Therefore, it may be possible to extend Z_{SD} mapping to archived satellite data, such as the Landsat series data.

5.3. Key factors related to spatial patterns of lake clarity across China

Our results show that there is a distinct "high west and low east" spatial pattern and overall ever-increasing water clarity in the past two decades across China. Although several lakes experienced a significant decrease in water clarity, such as Qinghai Lake and Hulun Lake, more lakes tended to increase. Agreeing with our results, previous studies have shown that lake water quality has increased in China during the last twenty years (Feng et al., 2019a; Zhou et al., 2019), although no studies have investigated nationwide changes in lake water clarity.

To explore the environmental factors that relate to the spatial patterns of lake clarity across China, we examined the relationships between the mean climatological summer Z_{SD} and local environmental factors. The results showed that both lake AL and WD had a significant positive correlation with the mean summer Z_{SD} (R^2 = 0.31 and 0.58, respectively), as lakes in west China generally have higher altitude and deeper water compared with those in east China. More importantly, deep waters are unlikely affected by bottom sediment resuspension events (Binding et al., 2015). Lake SA did not have a significant correlation with water clarity. A small number of large lakes in east China are eutrophic and turbid, such as Taihu Lake, Chaohu Lake, and Xingkai Lake, while large lakes in west China, such as Namco Lake and Selingco Lake, are quite clear (Li et al., 2016).

Local AT and PR showed significant negative correlations with the mean climatological summer Z_{SD} (R^2 = 0.26 and 0.15, respectively), suggesting that turbid lakes are common in areas of high temperature and precipitation throughout China, such as the middle and lower reaches of the Yangtze River in the EPR. This is in consistent with previous studies which have illustrated that high air temperature may promote algal growth and then decrease water clarity (Chen et al., 2013; Zhou et al., 2019), while more precipitation may cause more sediment and nutrient loadings into lakes (Rose et al., 2017). In contrast, no significant correlations were found among WS, NDVI, and the mean summer Z_{SD}, illustrating that these parameters are not the main factors that affect the water clarity spatial patterns across China. For the anthropogenic factors, the mean climatological summer Z_{SD} had a negative correlation with local PO and GDP (R^2 = 0.26 and 0.20, respectively), suggesting that lakes in provinces with high population and GDP tend to be turbid. This agrees well with previous studies (Cao et al., 2017; Borkman and Smayda, 1998) as population and GDP are indicators of anthropogenic interference. In general, the distinct high west and low east pattern in water clarity was found to be associated with the apparent differences in water depth, altitude, air temperature, precipitation, GDP, and population in west versus east China, separated by the H-T line, as shown in Fig. 14. Lake geographic factors, such as water depth and lake altitude, are the likely leading factors for this spatial pattern while meteorological and anthropogenic factors also contribute to a certain degree.

5.4. Correlations between the long-term lake clarity change and regional climate variables

Significant changes in global climate have been observed over the past century and imposed direct and indirect impacts on lake ecosystems through the hydrological cycle (Bates et al., 2008). Changes in temperature, precipitation, wind, glaciers, and snow cover have been documented as drivers of water quality dynamics and water pollution via nutrients, sediments, dissolved organic carbon, pathogens, pesticides, and salt (O'Reilly et al., 2003). However, our understanding of the effects that climate variables have on both aquatic ecosystem functions and water clarity across large regions remains limited.

To preliminarily explore the responses of lake clarity interannual variability to climate change from 2000 to 2017, we conducted correlation analyses between the long-term mean summer Z_{SD} and local meteorological factors (i.e. AT, PR, and WS), together with corresponding lake geographic factor (i.e., lake SA). Lake depth was not considered here due to the lack of long-term data for these two parameters. But studies have shown that changes in lake water depth or water level have a direct link with changes in lake surface area (Wu et al., 2019), such that changes in the lake SA can also represent, to a certain extent, the changes in the water level. As shown in Fig. 15,

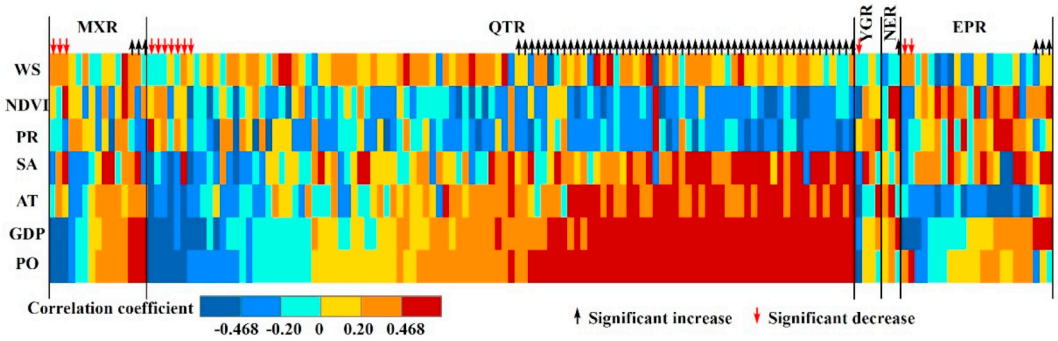

Fig. 15. A heat map showing the Pearson correlation coefficients between long-term Z_{SD} and potential environmental factors for the large lakes ($N = 153$) across China in the five lake regions. Note that when the correlation coefficient is larger than o.468 or smaller than −0.468, the correlation is significant ($p < .05$). WS denotes wind speed, PR denotes precipitation, NDVI denotes normalized difference vegetation index, SA denotes lake surface area, AT denotes air temperature, GDP denotes gross domestic production, and PO denotes population. Lake Z_{SD} with significant increases and decreases from 2000 to 2017 are marked.

stronger correlations were observed between changes in the long-term water clarity and AT and SA. Correlation coefficients were generally weaker for WS, PR, and NDVI. The overall correlations between these factors and changes in the interannual water clarity also varied across the five lake regions. We note that Fig. 17 also showed the correlations between lake clarity and anthropogenic factors (GDP and PO), but these two factors were not considered for lakes in the QTR and MXR, where human activity is generally weak.

In the 52 lakes with significant increasing Z_{SD} in QTR, most of the lakes had positive correlations with both AT and SA. Moreover, 30 of the 52 lakes had significant positive correlations with AT, and 24 of them had significant positive correlations with SA, suggesting the positive effect of the two factors on lake clarity change in QTR. Studies have shown that climate warming have resulted in water level rise at lakes in QTR due to increasing meltwater from glaciers and permafrost in the cold regions (Wan et al., 2018; Zhang et al., 2011). Water level rise then would lead to the increase in water clarity by diluting the dissolved and suspended matter in lakes (Li et al., 2016). Fig. S4 in the Supplementary Material showed the long-term changes in water clarity in Lake Namco, along with the variations in the water level (acquired from Wu et al., 2019), SA, and AT, which further confirmed that the rise in the water level is associated with the increase of temperature. In contrast, in the 7 lakes with significant decreasing trend in QTR, most of them had negative correlations with AT and SA. This is probably due to the sediments carried by meltwater that will decrease the lake clarity, such as the case in Lake Silingco (Mi et al., 2019). Alternatively, the lake clarity may be impacted by higher temperature which can accelerate the growth of phytoplankton in relative warm area of QTR, such as the case in Lake Qinghai (Feng et al., 2019b).

In MXR, SA had significant positive correlations with 4 lakes including 1 with significant decreasing trend and 1 with significant increasing trend, implying lake clarity is usually positively linked to water level of the lake in this region.

In the east (including EPR, YGR and NER), AT generally had negative correlations with most lakes, among which 9 lakes were significant negatively correlated, which is consistent with previous studies that high temperature can accelerate the growth of phytoplankton and result in decreases in the water clarity in many lakes in east China (Chen et al., 2013; Zhou et al., 2019). But these significant correlated lakes were not those had significant changing trend in water clarity, illustrating other factors may have larger effect on lake clarity in the east, such as GDP and PO which will be analyzed in Section 5.5. SA also generally had positively correlations with lake clarity in the east, among which significant 7 lakes were significant positively correlated. Besides, NDVI showed significant positive correlations with water clarity change in 9 lakes in EPR and NER, which was explained in relevant studies that the vegetation cover may reduce the suspended sediment discharged into lakes (Feng et al., 2019a).

5.5. Correlations between the long-term lake clarity change and regional anthropogenic variables

After the 1970s, China has experienced rapid industrialization, urbanization, and population expansion during the last half-century, especially in east China. On one hand, the socioeconomic development has caused a series of water quality degradation and pollution issues, which have been documented in many studies in China, such as the frequent algal blooms in Chaohu Lake and Taihu Lake starting from the late 1980s especially in 2007, and continuous algal blooms in Dianchi Lake around 2000 (Chen et al., 2013; Gao and Yan, 2002; Hu et al., 2010; Huang and Shu, 1997; Le et al., 2010; Zhang et al., 1999; Zhao et al., 2018). On the other hand, to control the water pollution, a full range of forceful regulation and water treatment projects have been taken by local and national governments in China mainly after 2000s with billions of money invested (Meng et al., 2015; Zhou, 2010). Hence, the correlations between the human activity factors, i.e. GDP and PO, and the lake clarity change between 2000 and 2017 were discussed below to preliminarily reveal the general relationship between economic development and lake quality change in the past two decades in the east China.

As shown in Fig. 15, we found 63.3% of the lakes showed positive correlations with local GDP growth in EPR, NER and YGR, and all the 4 lakes with significant increasing trend in water clarity had significant positive correlations with local GDP growth. However, there were ~ 25% lakes whose clarity had negative correlations with GDP growth in east China, in which all the 3 lakes with significant decreasing trend in water clarity in the east had significant negative correlations with the GDP growth, illustrating the negative effect of local GDP growth on lake clarity change in some regions in the east.

Fig. 16 shows three examples of lake in the EPR with the long-term changing curves of the mean summer Z_{SD} and the major correlated factors. These three aquatic systems (including the Danjiangkou Reservoir, Suyahu Reservoirs and Nanyin Reservoir) are reservoirs that operate as drinking water resources for local municipalities. In Suyahu Reservoir, a sudden increase of lake Z_{SD} was found from 2009 to 2012, which appeared to be related to the environmental management and forced shutdown of heavily polluting industries by the local government (http://henan.people.com.cn/n2/2017/0126/c351638-29648322.html). In Danjiangkou Reservoir, Fig. 19(b) shows that SA followed the changes of lake Z_{SD}, with a sharp increase for both the Z_{SD} and SA between 2014 and 2015, which further support that the SA is acting as a proxy for the dilution process associated with water level rise. This is likely due to the opening of the South–North Water Transfer Project central route in December 2014 (Lei et al., 2018). In Nanyin Reservoir, fluctuations in Z_{SD} between 2007 and 2010 appeared to be related to the reinforcement project initiated in Nanyin Reservoir during this period (Jiang and Zheng, 2011), and it can be seen that the water Z_{SD} remained at a higher

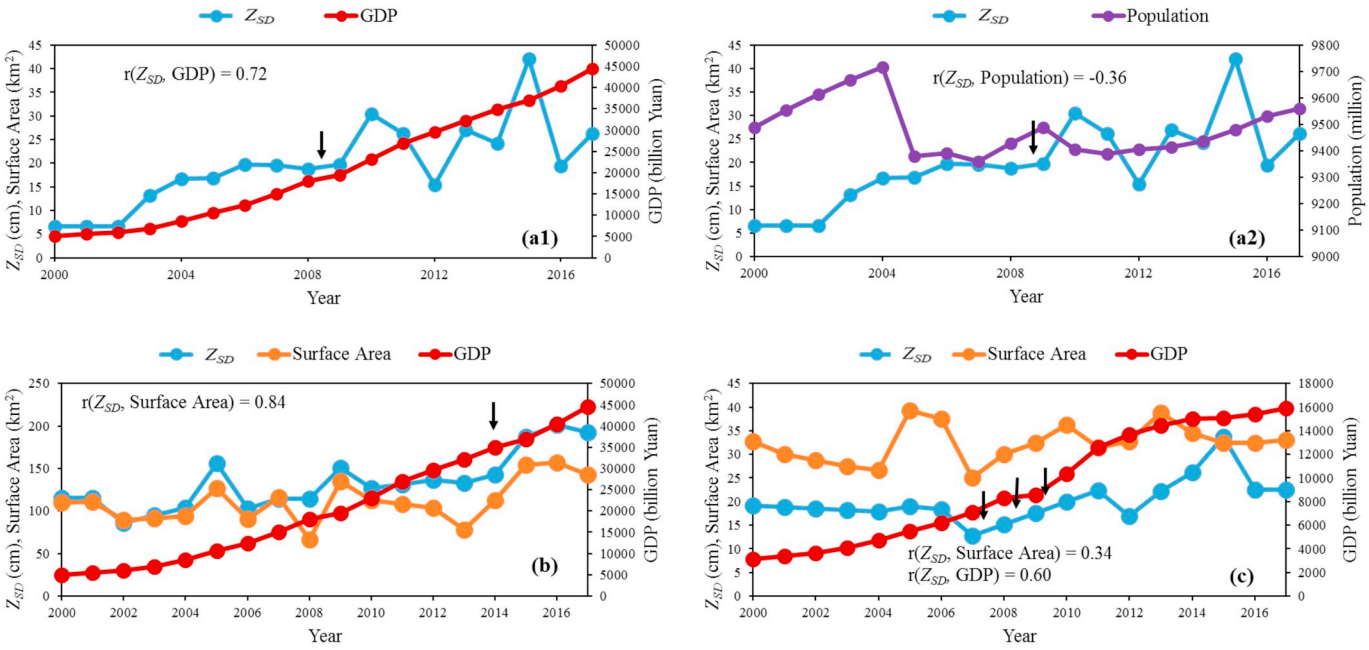

Fig. 16. Long-term change curves and Pearson correlation coefficients (r) between lake Z_{SD} and local influencing environmental factors for lakes with significantly increasing Z_{SD}: (a) Suyahu Reservoir in the EPR, (b) Danjiangkou Reservoir (Henan Province part) in the EPR, and (c) Nanyin Reservoir in the NER. The major water management measures for these reservoirs are denoted with black arrows at their time of deployment. We note that the SA data here has subtracted the area of the 500 m-buffer inward of the water boundary in MODIS.

level after 2010.

In general, these implies the effectiveness of water quality regulation for lakes in east China, and give evidence of GDP growth's positive role on lake clarity increase in industrializing and urbanizing areas through supporting effective water resource management and pollution control measures, although this effect is indirect and relying on the good governance and balance of industrialization and environmental management. Agreeing with our results, recent studies have recognized the signs of water quality recovery in several Chinese lakes as a result of continuous treatment and management supported by local and national governments (Guo et al., 2015; He et al., 2015; Feng et al., 2019a; Zhao et al., 2018). But we found these lakes with significantly increasing trend were generally small reservoirs, which means the regulation and management deployed for reservoirs were stronger than that for natural lakes. Besides, a small portion of lakes (~25%), including the 3 significant decreasing lakes in the east, were still negatively impacted by the local GDP growth, suggesting effective water managements are still required in some area.

For the factor of PO, it was positively correlated with the lake clarity change in most lakes, but the effect of local PO on lake clarity seems vague and not obvious. We note that climate, lake water, biophysical, and socio-economic systems are interconnected in complex ways (Maberly and Elliott, 2012; Williamson et al., 2009). Our study just provides preliminary analyses and discussions on the simple correlations between climate change and human activity on regional lake clarity. Systematic interactions and responses of water quality in regional and global lakes to climatic and anthropogenic changes remain to be studied in future studies by bridging the gap between water color satellite remote sensing and biogeochemical/ecosystem modelling (IOCCG, 2020).

6. Concluding remarks

In this study, we developed and validated an FUI and α-based model to estimate Z_{SD} for large lakes across China based on in-situ measurements and synchronous MODIS imagery. Compared with other empirical Z_{SD} models, this FUI and α-based model demonstrates superior performance (MRD = 27.4%) and adaptability for lakes over a wide range of clarity and trophic states. This benefits from the stable and satisfactory relationship between water color (i.e., FUI and α) and Z_{SD} over a wide range, supported by both in-situ and simulation datasets.

Subsequently, the spatial patterns and long-term variations in Z_{SD} for large lakes (N = 153) across China from 2000 to 2017 were investigated and recognized using MODIS with the proposed model. Based on the MODIS retrieved results, a spatial pattern of "high west and low east" was observed for the lakes across China, with an ever-increasing pattern in water clarity from 2000 to 2017 for the majority of the lakes, especially in west China. It was found that the average annual change rate of all lakes was 3.3 cm/yr, where 38.6% (N = 59) of the lakes experienced a significant increase in water clarity during the past eighteen years, whereas only 8.5% (N = 13) of the lakes had a significantly decreasing trend. Furthermore, the environmental factors that may potentially affect this spatio-temporal pattern were preliminarily analyzed and discussed in terms of the correlations between Z_{SD} and lake geographic, local climate, and anthropogenic factors. Spatially, the variation patterns in lake clarity across China was found to be associated with distinct differences in lake depth and altitude between east and west China while air temperature, precipitation, population, and GDP distribution also contributed to a certain extent. Temporally, it showed that changes in the lake surface area and water level are possibly the direct factors that drive changes in lake clarity. In west China, the dramatic increase of lake clarity was observed to be positively correlated to the increase of the water surface area which is linked to climate warming. In east China, however, the small overall increases of lake clarity might be influenced by the combined effects of vegetation cover growth, climate warming and water resource management over recent decades. Specifically, we found that GDP growth generally showed positive correlations with increases in water clarity in most lakes in east China, which implied the effectiveness of water management practices that had already been enacted. The results of this study provide important information for water quality conservation and management in China, and highlight the value of satellite remote sensing in monitoring water quality over lakes at broad scales and over long term.

Acknowledgements

We would like to thank Dr. Liping Zhu and Mr. Chong Liu for providing the in situ data from Tibetan Plateau lakes, and Dr. Lian Feng, Dr. Hongtao Duan, Dr. Kaishan Song, Dr. Liming Jia for providing in situ data from some other lakes for validation. We also thank the three anonymous reviewers and the editorial staff for their valuable and helpful comments. This study was jointly funded by the National Key Research and Development Program of China (2017YFC0405804), National Natural Science Foundation of China (41901272, 41971318), and China Postdoctoral Science Foundation (8206300163).

Declaration of Competing Interest

The authors declare that they have no known competing financial interests or personal relationships that could have appeared to influence the work reported in this paper.

Appendix A. Supplementary data

Supplementary data to this article can be found online at https://doi.org/10.1016/j.rse.2020.111949.

References

Adrian, R., O'Reilly, C.M., Zagarese, H., Baines, S.B., Hessen, D.O., Keller, W., Livingstone, D.M., Sommaruga, R., Straile, D., Van Donk, E., Weyhenmeyer, G.A., 2009. Lakes as sentinels of climate change. Limnol. Oceanogr. 54 (6part2), 2283–2297.

Bates, B., Kundzewicz, Z., Wu, S., 2008. Climate Change and Water. Intergovernmental Panel on Climate Change Secretariat.

Biber, P.D., Paerl, H.W., Gallegos, C.L., Kenworthy, W.J., 2005. Evaluating Indicators of Seagrass Stress to Light. (Estuarine indicators).

Binding, C.E., Jerome, J.H., Bukata, R.P., Booty, W.G., 2007. Trends in water clarity of the lower Great Lakes from remotely sensed aquatic color. J. Great Lakes Res. 33 (4), 828–841.

Binding, C.E., Greenberg, T.A., Watson, S.B., Rastin, S., Gould, J., 2015. Long term water clarity changes in North America's Great Lakes from multi-sensor satellite observations. Limnol. Oceanogr. 60 (6), 1976–1995.

Borkman, D.G., Smayda, T.J., 1998. Long-term trends in water clarity revealed by Secchi-disk measurements in lower Narragansett Bay. ICES J. Mar. Sci. 55 (4), 668–679.

Cao, Z., Duan, H., Feng, L., Ma, R., Xue, K., 2017. Climate-and human-induced changes in suspended particulate matter over Lake Hongze on short and long timescales. Remote Sens. Environ. 192, 98–113.

Chen, X., Yang, X., Dong, X., Liu, E., 2013. Environmental changes in Chaohu Lake (southeast, China) since the mid 20th century: the interactive impacts of nutrients, hydrology and climate. Limnol. Ecol. Manag. Inland Waters 43 (1), 10–17.

de Eyto, E., Jennings, E., Ryder, E., Sparber, K., Dillane, M., Dalton, C., Poole, R., 2016. Response of a humic lake ecosystem to an extreme precipitation event: physical, chemical, and biological implications. Inland Waters 6 (4), 483–498.

Dörnhöfer, K., Oppelt, N., 2016. Remote sensing for lake research and monitoring–recent advances. Ecol. Indic. 64, 105–122.

Doron, M., Babin, M., Hembise, O., Mangin, A., Garnesson, P., 2011. Ocean transparency from space: validation of algorithms estimating Secchi depth using MERIS, MODIS and SeaWiFS data. Remote Sens. Environ. 115 (12), 2986–3001.

Duan, H., Ma, R., Zhang, Y., Zhang, B., 2009. Remote-sensing assessment of regional inland lake water clarity in Northeast China. Limnology 10 (2), 135.

Duan, H., Loiselle, S.A., Zhu, L., Feng, L., Zhang, Y., Ma, R., 2015. Distribution and incidence of algal blooms in Lake Taihu. Aquat. Sci. 77 (1), 9–16.

Farr, T.G., Rosen, P.A., Caro, E., Crippen, R., Duren, R., Hensley, S., Kobrick, M., Paller, M., Rodriguez, E., Roth, L., Seal, D., 2007. The shuttle radar topography mission. Rev. Geophys. 45 (2).

Feng, L., Hu, C., Li, J., 2018a. Can MODIS land reflectance products be used for estuarine and inland waters? Water Resour. Res. 54 (5), 3583–3601.

Feng, L., Hou, X., Li, J., Zheng, Y., 2018b. Exploring the potential of Rayleigh-corrected reflectance in coastal and inland water applications: a simple aerosol correction method and its merits. ISPRS J. Photogramm. Remote Sens. 146, 52–64.

Feng, L., Hou, X., Zheng, Y., 2019a. Monitoring and understanding the water transparency changes of fifty large lakes on the Yangtze plain based on long-term MODIS observations. Remote Sens. Environ. 221, 675–686.

Feng, L., Liu, J., Ali, T.A., Li, J., Li, J., Kuang, X., 2019b. Impacts of the decreased freeze-up period on primary production in Qinghai Lake. Int. J. Appl. Earth Obs. Geoinf. 83, 101915.

Gao, L.Q., Yan, W.J., 2002. Eutrophication of China's three lakes: current situation and countermeasures. Resour. Sci. 24 (3), 19–25.

Garaba, S., Friedrichs, A., Voß, D., Zielinski, O., 2015. Classifying natural waters with the Forel-Ule colour index system: results, applications, correlations and crowdsourcing. Int. J. Environ. Res. Public Health 12 (12), 16096–16109.

Ge, M.L., Feng, Z.M., 2008. Study of China's 2000 population distribution pattern based on GIS: and contrast with the population of Hu Huanyong line in 1935. Popul. Res. 32 (1), 51–57.

Guo, Y., Zhao, Y., Long, S., et al., 2015. Study on characteristics of water environment in the stage of lake eutrophication treatment: a case study of Hongfeng Lake, a drinking water source in Guiyang City. Environ. Pollut. Control (6), 55.

He, J., Xu, X., Yang, Y., Wu, X., Wang, L., Li, S., Zhou, H., 2015. Problems and effects of comprehensive management of water environment in Lake Dianchi. J. Lake Sci. 27 (2), 195–199.

He, J., Yang, K., Tang, W., Lu, H., Qin, J., Chen, Y.Y., Li, X., 2020. The first high-resolution meteorological forcing dataset for land process studies over China. Sci. Data 7 (25). https://doi.org/10.1038/s41597-020-0369-y.

Hou, X., Feng, L., Duan, H., Chen, X., Sun, D., Shi, K., 2017. Fifteen-year monitoring of the turbidity dynamics in large lakes and reservoirs in the middle and lower basin of the Yangtze River, China. Remote Sens. Environ. 190, 107–121.

Hu, H., 1990. The distribution, regionalization and prospect of China's population (in Chinese). Sci. Geogr. Sin. 45 (2), 139–144.

Hu, C., 2009. A novel ocean color index to detect floating algae in the global oceans. Remote Sens. Environ. 113 (10), 2118–2129.

Hu, C., Lee, Z., Ma, R., Yu, K., Li, D., Shang, S., 2010. Moderate resolution imaging spectroradiometer (MODIS) observations of cyanobacteria blooms in Taihu Lake, China. J. Geophys. Res Oceans (C4), 115.

Huang, W., Shu, J., 1997. Eutrophication evaluation of major reservoirs in China. in Chinese. Guizhou Environ. Protection Technology 3 (2), 12–16.

IOCCG, 2006. Remote sensing of inherent optical properties: fundamentals, tests of algorithms, and applications. In: Lee, Z.-P. (Ed.), Reports of the International Ocean-Colour Coordinating Group, No. 5. International Ocean Colour Coordinating Group, Dartmouth, Canada.

IOCCG, 2018. Earth observations in support of global water quality monitoring. In: Greb, S., Dekker, A., Binding, C. (Eds.), IOCCG Report Series, No. 17. International Ocean Colour Coordinating Group, Dartmouth, Canada.

IOCCG, 2020. Synergy between Ocean Colour and biogeochemical/ecosystem models. In: Dutkiewicz, S. (Ed.), IOCCG Report Series, No. 19. International Ocean Colour Coordinating Group, Dartmouth, Canada.

Jiang, X., Zheng, K., 2011. Brief discussion on new ways of comprehensive development and utilization of water resources in Nanxun reservoir (in Chinese). Water Technol. Econ. 17 (1), 81–82.

Kirk, J.T., 1994. Light and Photosynthesis in Aquatic Ecosystems. Cambridge university press.

Kratzer, S., Brockmann, C., Moore, G., 2008. Using MERIS full resolution data to monitor coastal waters - A case study from Himmerfjarden, a fjord-like bay in the north-western Baltic Sea. Remote Sens. Environ. 112 (5), 2284–2300 In press.

Le, C., Zha, Y., Li, Y., Sun, D., Lu, H., Yin, B., 2010. Eutrophication of lake waters in China: cost, causes, and control. Environ. Manag. 45 (4), 662–668.

Lee, Z., Shang, S., Hu, C., Du, K., Weidemann, A., Hou, W., Lin, J., Lin, G., 2015. Secchi disk depth: a new theory and mechanistic model for underwater visibility. Remote Sens. Environ. 169, 139–149.

Lee, Z., Shang, S., Qi, L., Yan, J., Lin, G., 2016. A semi-analytical scheme to estimate Secchi-disk depth from Landsat-8 measurements. Remote Sens. Environ. 177, 101–106.

Lee, Z., Arnone, R., Boyce, D., Franz, B., Greb, S., Hu, C., Lavender, S., Lewis, M., Schaeffer, B., Shang, S., Wang, M., 2018a. Global water clarity: continuing a century-long monitoring. Eos 99.

Lee, Z., Shang, S., Du, K., Wei, J., 2018b. Resolving the long-standing puzzles about the observed Secchi depth relationships. Limnol. Oceanogr. 63 (6), 2321–2336.

Li, J., Wang, S., Wu, Y., Zhang, B., Chen, X., Zhang, F., Shen, Q., Peng, D., Tian, L., 2016. MODIS observations of water color of the largest 10 lakes in China between 2000 and 2012. Int. J. Digital Earth 9 (8), 788–805.

Lehmann, M., Nguyen, U., Allan, M., Van der Woerd, H., 2018. Colour Classification of 1486 Lakes across a Wide Range of Optical Water Types. Remote Sensing 10 (8).

Li, J., Hu, C., Shen, Q., Barnes, B.B., Murch, B., Feng, L., Zhang, M., Zhang, B., 2017. Recovering low quality MODIS-Terra data over highly turbid waters through noise reduction and regional vicarious calibration adjustment: a case study in Taihu Lake. Remote Sens. Environ. 197, 72–84.

Liu, C., Zhu, L., Wang, J., Qiao, B., Ju, J., Huang, L., 2017. Remote sensing-based estimation of lake water clarity on the Tibetan plateau. Prog. Geogr. 36 (5), 597–609.

Ma, R., Duan, H., Hu, C., Feng, X., Li, A., Ju, W., Jiang, J., Yang, G., 2010. A half-century of changes in China's lakes: global warming or human influence? Geophys. Res. Lett. 37 (24).

Ma, R., Yang, G., Duan, H., Jiang, J., Wang, S., Feng, X., Li, A., Kong, F., Xue, B., Wu, J., Li, S., 2011. China's lakes at present: number, area and spatial distribution. Sci. China Earth Sci. 54 (2), 283–289.

Maberly, S.C., Elliott, J.A., 2012. Insights from long-term studies in the Windermere catchment: external stressors, internal interactions and the structure and function of lake ecosystems. Freshw. Biol. 57 (2), 233–243.

McCullough, I.M., Loftin, C.S., Sader, S.A., 2012. Combining lake and watershed characteristics with Landsat TM data for remote estimation of regional lake clarity. Remote Sens. Environ. 123, 109–115.

McPherson, M.L., Hill, V.J., Zimmerman, R.C., Dierssen, H.M., 2011. The optical properties of greater Florida bay: implications for seagrass abundance. Estuar. Coasts 34 (6), 1150.

Meng, X., Zhang, Y., Yu, X., Zhan, J., Chai, Y., Critto, A., et al., 2015. Analysis of the temporal and spatial distribution of Lake and reservoir water quality in China and changes in its relationship with GDP from 2005 to 2010. Sustainability 7 (2), 2000–2027.

Mi, H., Fagherazzi, S., Qiao, G., Hong, Y., Fichot, C.G., 2019. Climate change leads to a

doubling of turbidity in a rapidly expanding Tibetan lake. Sci. Total Environ. 688, 952–959.
Mouw, C.B., Greb, S., Aurin, D., DiGiacomo, P.M., Lee, Z., Twardowski, M., Binding, C., Hu, C., Ma, R., Moore, T., Moses, W., 2015. Aquatic color radiometry remote sensing of coastal and inland waters: challenges and recommendations for future satellite missions. Remote Sens. Environ. 160, 15–30.
Mueller, J.L., Morel, A., Frouin, R., Davis, C., Arnone, R., Carder, K., Lee, Z.P., Steward, R.G., Hooker, S., Mobley, C.D., McLean, S., 2003. Ocean Optics Protocols for Satellite Ocean Color Sensor Validation, Revision 4. Volume III: Radiometric Measurements and Data Analysis Protocols.
Neil, C., Spyrakos, E., Hunter, P.D., Tyler, A.N., 2019. A global approach for chlorophyll-a retrieval across optically complex inland waters based on optical water types. Remote Sens. Environ. 229, 159–178.
Novoa, S., Wernand, M.R., Van der Woerd, H.J., 2013. The Forel-Ule scale revisited spectrally: preparation protocol, transmission measurements and chromaticity. J. Euro. Opt. Soc. Rapid Publ. 8.
Olmanson, L.G., Bauer, M.E., Brezonik, P.L., 2008. A 20-year Landsat water clarity census of Minnesota's 10,000 lakes. Remote Sens. Environ. 112 (11), 4086–4097.
Olmanson, L.G., Brezonik, P.L., Finlay, J.C., Bauer, M.E., 2016. Comparison of Landsat 8 and Landsat 7 for regional measurements of CDOM and water clarity in lakes. Remote Sens. Environ. 185, 119–128.
O'Reilly, C.M., Alin, S.R., Plisnier, P.D., Cohen, A.S., McKee, B.A., 2003. Climate change decreases aquatic ecosystem productivity of Lake Tanganyika, Africa. Nature 424 (6950), 766.
Palmer, S.C., Kutser, T., Hunter, P.D., 2015. Remote sensing of inland waters: challenges, progress and future directions. Remote Sens. Environ. 157, 1–8.
Pirhalla, D.E., Sheridan, S.C., Lee, C.C., Barnes, B.B., Ransibrahmanakul, V., Hu, C., 2017. Water clarity patterns in South Florida coastal waters and their linkages to synoptic-scale wind forcing. Satell. Oceanogr. Meteorol. 2 (1), 26–40.
Pitarch, J., van der Woerd, H.J., Brewin, R.J., Zielinski, O., 2019. Optical properties of Forel-Ule water types deduced from 15 years of global satellite ocean color observations. Remote Sens. Environ. 231, 111249.
Ren, J., Zheng, Z., Li, Y., Lv, G., Wang, Q., Lyu, H., Huang, C., Liu, G., Du, C., Mu, M., Lei, S., 2018. Remote observation of water clarity patterns in three gorges reservoir and Dongting Lake of China and their probable linkage to the three gorges dam based on Landsat 8 imagery. Sci. Total Environ. 625, 1554–1566.
Rodrigues, T., Alcântara, E., Watanabe, F., Imai, N., 2017. Retrieval of Secchi disk depth from a reservoir using a semi-analytical scheme. Remote Sens. Environ. 198, 213–228.
Rose, K.C., Greb, S.R., Diebel, M., Turner, M.G., 2017. Annual precipitation regulates spatial and temporal drivers of lake water clarity. Ecol. Appl. 27 (2), 632–643.
Shen, Q., Yao, Y., Li, J., Zhang, F., Wang, S., et al., 2019. A CIE Color Purity Algorithm to Detect Black and Odorous Water in Urban Rivers Using High-Resolution Multispectral Remote Sensing Images. IEEE Transactions on Geoscience and Remote Sensing 57 (9), 6577–6590.
Shi, K., Zhang, Y., Zhu, G., Qin, B., Pan, D., 2018. Deteriorating water clarity in shallow waters: evidence from long term MODIS and in-situ observations. Int. J. Appl. Earth Obs. Geoinf. 68, 287–297.
Spyrakos, E., O'Donnell, R., Hunter, P.D., Miller, C., Scott, M., Simis, S.G., Neil, C., Barbosa, C.C., Binding, C.E., Bradt, S., Bresciani, M., 2018. Optical types of inland and coastal waters. Limnol. Oceanogr. 63 (2), 846–870.
Srebotnjak, T., Carr, G., de Sherbinin, A., Rickwood, C., 2012. A global water quality index and hot-deck imputation of missing data. Ecol. Indic. 17, 108–119.
Suominen, T., Tolvanen, H., 2016. Temporal analysis of remotely sensed turbidity in a coastal archipelago. Int. J. Appl. Earth Obs. Geoinf. 49, 188–199.
Tyler, A.N., Hunter, P.D., Spyrakos, E., Groom, S., Constantinescu, A.M., Kitchen, J., 2016. Developments in earth observation for the assessment and monitoring of inland, transitional, coastal and shelf-sea waters. Sci. Total Environ. 572, 1307–1321.
Van der Woerd, H., Wernand, M., 2018. Hue-angle product for low to medium spatial resolution optical satellite sensors. Remote Sens. 10 (2), 180.
Vermote, E.F., 2015. MOD09A1 MODIS Surface Reflectance 8-Day L3 Global 500m SIN Grid V006. NASA EOSDIS Land Processes DAAC.
Vermote, E.F., Kotchenova, S.Y., 2008. MOD09 (Surface Reflectance) User's Guide, Version 1.1, March. 2008. Greenbelt, MD.
Wan, W., Zhao, L., Xie, H., Liu, B., Li, H., Cui, Y., Ma, Y., Hong, Y., 2018. Lake surface water temperature change over the Tibetan plateau from 2001 to 2015: a sensitive indicator of the warming climate. Geophys. Res. Lett. 45 (20), 11–177.
Wang, S.M., Dou, H.S., 1998. Chinese Lake Catalogue (in Chinese). Science Press, Beijing.
Wang, S., Li, J., Shen, Q., Zhang, B., Zhang, F., Lu, Z., 2015. MODIS-based radiometric color extraction and classification of inland water with the Forel-Ule scale: a case study of lake Taihu. IEEE J. Sel. Topics Appl. Earth Obs. Remote Sens. 8 (2), 907–918.
Wang, S., Li, J., Zhang, B., Spyrakos, E., Tyler, A.N., Shen, Q., et al., 2018. Trophic state assessment of global inland waters using a MODIS-derived Forel-Ule index. Remote Sens. Environ. 217, 444–460 In press.
Wang, M., Shi, W., Tang, J., 2011. Water property monitoring and assessment for China's inland Lake Taihu from MODIS-aqua measurements. Remote Sens. Environ. 115 (3), 841–854.
Wang, S., Li, J., Junsheng, L., Zhang, B., Shen, Q., Zhang, F., Lu, Z., 2016. A simple correction method for the MODIS surface reflectance product over typical inland waters in China. Int. J. Remote Sens. 37 (24), 6076–6096.
Wernand, M.R., 2010. On the history of the Secchi disc. J. Euro. Opt. Soc. Rapid Publ. 5.
Wernand, M.R., Hommersom, A., van der Woerd, H.J., 2013. MERIS-Based Ocean colour classification with the discrete Forel-Ule scale. Ocean Sci. Discuss. 9, 2817–2849.
Williamson, C.E., Saros, J.E., Vincent, W.F., Smol, J.P., 2009. Lakes and reservoirs as sentinels, integrators, and regulators of climate change. Limnol. Oceanogr. 54 (6part2), 2273–2282.
Wu, G., De Leeuw, J., Skidmore, A.K., Prins, H.H., Liu, Y., 2008. Comparison of MODIS and Landsat TM5 images for mapping tempo–spatial dynamics of Secchi disk depths in Poyang Lake National Nature Reserve, China. Int. J. Remote Sens. 29 (8), 2183–2198.
Wu, Y., Li, M., Guo, L., Zheng, H., Zhang, H., 2019. Investigating water variation of lakes in Tibetan plateau using remote sensed data over the past 20 years. IEEE J. Sel. Top. Appl. Earth Obs. Remote Sens. (7), 2557–2564.
Yang, K., He, J., Tang, W., Qin, J., Cheng, C.C., 2010a. On downward shortwave and longwave radiations over high altitude regions: observation and modeling in the Tibetan plateau. Agric. For. Meteorol. 150 (1), 38–46.
Yang, G., Ma, R., Zhang, L., Jiang, J., Yao, S., Zhang, M., Zeng, H.D., 2010b. Lake status, major problems and protection strategy in China. J. Lake Sci. 22 (6), 799–810.
Zhang, Z., Wang, P., Zhang, C., 1999. Study on the eutrophication in Chaohu Lake and its remediation. Res. Environ. Sci./Huanjing Kexue Yanjiu 12 (5), 45–48.
Zhang, G., Xie, H., Kang, S., Yi, D., Ackley, S.F., 2011. Monitoring lake level changes on the Tibetan plateau using ICESat altimetry data (2003–2009). Remote Sens. Environ. 115 (7), 1733–1742.
Zhang, G., Yao, T., Chen, W., Zheng, G., Shum, C.K., Yang, K., Piao, S., Sheng, Y., Yi, S., Li, J., O'Reilly, C.M., 2019. Regional differences of lake evolution across China during 1960s–2015 and its natural and anthropogenic causes. Remote Sens. Environ. 221, 386–404.
Zhao, D., Li, J., Hu, R., Shen, Q., Zhang, F., 2018. Landsat-satellite-based analysis of spatial–temporal dynamics and drivers of CyanoHABs in the plateau Lake Dianchi. Int. J. Remote Sens. 39 (23), 8552–8571.
Zhou, Q., 2010. Research and comprehensive demonstration of urban water pollution control and water environment control Technology in Chaohu Lake Basin (in Chinese). Constr. Technol. 3, 24–25.
Zhou, T., Wu, J., Peng, S., 2012. Assessing the effects of landscape pattern on river water quality at multiple scales: a case study of the Dongjiang River watershed, China. Ecol. Indic. 23, 166–175.
Zhou, Q., Wang, W., Huang, L., Zhang, Y., Qin, J., Li, K., Chen, L., 2019. Spatial and temporal variability in water transparency in Yunnan plateau lakes, China. Aquat. Sci. 81 (2), 36.
Zibordi, G., Berthon, J.F., Mélin, F., D'Alimonte, D., Kaitala, S., 2009. Validation of satellite ocean color primary products at optically complex coastal sites: northern Adriatic Sea, northern Baltic proper and gulf of Finland. Remote Sens. Environ. 113 (12), 2574–2591.